Mon. Not. R. Astron. Soc. **384,** 420–439 (2008) doi:10.1111/j.1365-2966.2007.12723.x

Image decomposition of barred galaxies and AGN hosts

Dimitri Alexei Gadotti★
Max-Planck-Institut für Astrophysik, Karl-Schwarzschild-Str. 1, D-85748 Garching bei München, Germany

Accepted 2007 November 14. Received 2007 November 12; in original form 2007 August 21

ABSTRACT

I present the results of multicomponent decomposition of *V* and *R* broad-band images of a sample of 17 nearby galaxies, most of them hosting bars and active galactic nuclei (AGN). I use BUDDA v2.1 to produce the fits, allowing the inclusion of bars and AGN in the models. A comparison with previous results from the literature shows a fairly good agreement. It is found that the axial ratio of bars, as measured from ellipse fits, can be severely underestimated if the galaxy axisymmetric component is relatively luminous. Thus, reliable bar axial ratios can only be determined by taking into account the contributions of bulge and disc to the light distribution in the galaxy image. Through a number of tests, I show that neglecting bars when modelling barred galaxies can result in an overestimation of the bulge-to-total luminosity ratio of a factor of 2. Similar effects result when bright, type 1 AGN are not considered in the models. By artificially redshifting the images, I show that the structural parameters of more distant galaxies can in general be reliably retrieved through image fitting, at least up to the point where the physical spatial resolution is $\approx$1.5 kpc. This corresponds, for instance, to images of galaxies at $z = 0.05$ with a seeing full width at half-maximum (FWHM) of 1.5 arcsec, typical of the Sloan Digital Sky Survey (SDSS). In addition, such a resolution is also similar to what can be achieved with the *Hubble Space Telescope* (*HST*), and ground-based telescopes with adaptive optics, at $z \sim$ 1–2. Thus, these results also concern deeper studies such as COSMOS and SINS. This exercise shows that disc parameters are particularly robust, but bulge parameters are prone to errors if its effective radius is small compared to the seeing radius, and might suffer from systematic effects. For instance, the bulge-to-total luminosity ratio is systematically overestimated, on average, by 0.05 (i.e. 5 per cent of the galaxy total luminosity). In this low-resolution regime, the effects of ignoring bars are still present, but AGN light is smeared out. I briefly discuss the consequences of these results to studies of the structural properties of galaxies, in particular on the stellar mass budget in the local Universe. With reasonable assumptions, it is possible to show that the stellar content in bars can be similar to that in classical bulges and elliptical galaxies. Finally, I revisit the cases of NGC 4608 and 5701 and show that the lack of stars in the disc region inside the bar radius is significant. Accordingly, the best-fitting model for the former uses a Freeman type II disc.

Key words: galaxies: bulges – galaxies: evolution – galaxies: formation – galaxies: fundamental parameters – galaxies: photometry – galaxies: structure.

1 INTRODUCTION

Parametric modelling of galaxy images has recently become a popular tool to measure structural parameters, such as scalelengths and stellar masses, of the different galactic components, particularly bulges and discs. Through this sort of analysis, one is also able to determine the relative importance of the bulge component, with parameters such as the bulge-to-total luminosity ratio B/T, one of the major attributes that define the Hubble sequence (Hubble 1926, 1936). It thus provides indispensable means to investigate the formation and evolution of galaxies, and the origin of the Hubble sequence, some of the key subjects in current astrophysical research. Such studies can be divided in two categories. In the first category, one usually finds samples of some tens of very nearby ($z < 0.01$) galaxies (e.g. de Jong 1995; Khosroshahi, Wadadekar & Kembhavi 2000; D'Onofrio 2001; Möllenhoff & Heidt 2001; Peng et al. 2002; de Souza, Gadotti & dos Anjos 2004; Laurikainen et al. 2004, 2006; Laurikainen, Salo & Buta 2005). In this case, it is possible to fit models on a more careful, individual basis, and study other components,

★E-mail: dimitri@mpa-garching.mpg.de

such as bars, lenses, rings and spirals, either by including them in the models or analysing residual images, where the fitted model is removed from the original galaxy image. In the second category, one usually finds samples of some hundreds or thousands of galaxies up to $z \sim 1$ (e.g. Marleau & Simard 1998; Tasca & White 2005; Allen et al. 2006; Häussler et al. 2007; Huertas-Company et al. 2007, see also Pignatelli, Fasano & Cassata 2006) where fits are done in an automated fashion and structural details are ignored, often smoothed out by the low physical spatial resolution. In this case, although individual fits might not be fully reliable, solid statistical analyses are attainable.

Studies in both categories provide observational constraints to test theoretical predictions from models or scenarios of galaxy formation and evolution. Consequently, in order not to hamper progress, it is critical to understand the weaknesses and biases of these techniques. In fact, image decomposition of galaxies is a complex and difficult endeavour. One has to define which components to fit, the model(s) to adopt, which code to use, or basically the algorithm in the search for the best fit, and the initial set-up for the fitting process. Furthermore, there are issues related to seeing effects, sky subtraction, crowding, spatial resolution and signal-to-noise ratio. Each one of these points affects the resulting physical parameters to some extent.

In this paper, I make a connection between the two categories and study some of the issues that might produce wrong results. First, I present the results of image decomposition of a sample of galaxies at $z \sim 0.005$. Most of these galaxies are barred and host active galactic nuclei (AGN), and these components are also fitted in the models. This provides structural parameters of bulges, bars and discs, and is particularly relevant, since it is in the study of galaxies with non-axisymmetric components like bars where two-dimensional (2D), image fitting is most advantageous over one-dimensional (1D), luminosity profile fitting. In addition, bars are known now to play a major role in galaxy evolution (e.g. Kormendy & Kennicutt 2004, and references therein) and thus a better understanding of this galactic component is needed. Then, I remove bars and AGN from the models and redo the fits to verify how harmful it may be to one's results not to include these components in the model when they are clearly present in the galaxy. This is motivated by the fact that most studies ignore bars, focusing on estimating the structural parameters of bulges and discs, even though bars are ubiquitous and can represent a significant fraction of a galaxy luminosity. In fact, Eskridge et al. (2000) find that only 27 per cent of a sample of 186 spiral galaxies is unbarred in the near-infrared (IR), and the fraction of the total luminosity of a galaxy in the bar can be as high as ∼30 per cent (see Sellwood & Wilkinson 1993). Furthermore, results in Laurikainen et al. (2005, 2006) hint that light from the bar can, at least in some cases, be attributed to the bulge if the bar is omitted in the model. In principle, this can also happen to the light from a bright AGN. Finally, I use artificially redshifted images of the galaxies in the sample to redo the fits and repeat the exercise of omitting bars and AGN. This allows me to check the effects of low resolution on the fits and the importance of having more detailed models when studying more distant galaxies.

This paper is organized as follows. In the next section, I briefly recall the relevant aspects of the data sample used here, referring the reader to Gadotti & de Souza (2006, hereafter GdS06), where one also finds a more detailed presentation of the acquisition and treatment of the raw data. In Section 3, I present the results from image decomposition with and without bars and AGN in the models, including a comparison with previous work. The corresponding results for the redshifted images are presented in Section 4. The implications of this work to studies based on image decomposition and structural analysis of galaxies are discussed in Section 5. I summarize and present the main conclusions in Section 6.

2 THE DATA

The sample consists of 17 disc galaxies selected in GdS06 at an average redshift of about 0.005. Basic data for these galaxies are displayed in Table 1. They are relatively bright, most are close to face-on, and have no strong morphological perturbations. These characteristics usually ensure a reliable structural analysis. This sample was selected to cover the various relevant properties of barred galaxies with morphological type earlier than Sbc. Only two galaxies have no clear bar in their images, although one of them is classified as weakly barred in de Vaucouleurs et al. (1991, hereafter RC3) and the others have bars which range from very weak to very strong features. For five galaxies (all classified as Seyferts) an AGN component is deemed necessary in the fitted model, but most of the galaxies in the sample are classified as having some type of AGN in the NASA/IPAC Extragalactic Database (NED). The positions in the Hubble sequence of the galaxies in the sample go from S0 to Sbc, according to the RC3. Thus, although this sample is not in any sense complete or unbiased, it has appropriate qualities to study the issues on image decomposition described in the Introduction, since it covers a suitable range of bulge, bar and AGN properties. This will become clearer below, with the results from the structural analysis, where one sees a relatively wide range of e.g. bulge and bar prominence, AGN luminosity and bar ellipticity and shape.

The images used in this work were obtained at the Kuiper 1.55-m telescope operated by the University of Arizona Steward Observatory, on Mount Bigelow. They were taken using Johnson–Morgan V and R broad-band filters, with a pixel size of 0.29 arcsec, and a square field of view of roughly 5 arcmin on a side. The total integration time was 1500 s in V and 900 s in R. The seeing full width at half-maximum (FWHM) was about 1.3 arcsec on average. Errors in the photometric calibrations are $\approx$0.02 mag, but not all nights were photometric. One could argue that a larger data set could be obtained, for instance, from the Sloan Digital Sky Survey (SDSS). It should be noted, however, that the images collected in GdS06 have a much higher signal-to-noise ratio, and were, on average, obtained under better seeing. In addition, the relatively small sample provides an opportunity to carefully check every decomposition performed, and assure that reliable results are obtained on an individual basis.

Further details on the properties of these galaxies, as well as on the observations and data reduction, can be found in GdS06. It is important to note that, for some of the galaxies, since they cover practically the whole field of view, a good estimate of the sky contribution was difficult to obtain. Likewise, in some cases, seeing measurements are not very accurate, since there were only a few stars in the field of view suitable for that. For these reasons, I excluded two galaxies from the original sample in GdS06, as well as all the B and I broad-band images, where the difficult sky subtraction might produce errors in the image decomposition. The inaccuracy in the seeing measurements, though, might not be too severe, as it was quite stable during the observing runs.

3 DECOMPOSITION OF ORIGINAL IMAGES

In this section, the results of image decomposition using the original images are presented. I will first describe relevant technical aspects of the method applied, and then show results using the

Table 1. Basic data for the galaxies in the sample.

Galaxy (1)	Type (2)	D_{25} (3)	$\log R_{25}$ (4)	m_B (5)	cz (6)	d (7)	AGN (8)
IC 0486	SBa	0.93	0.11	14.60	7792	111.3	Sey1
NGC 2110	SAB0	1.70	0.13		2064	29.5	Sey2
NGC 2911	SA0(s)	4.07	0.11	12.21	3195	45.6	Sey/LINER
NGC 3227	SABa(s)	5.37	0.17	11.59	1235	17.6	Sey1.5
NGC 4151	SABab(rs)	6.31	0.15	10.90	1190	17.0	Sey1.5
NGC 4267	SB0(s)	3.24	0.03	11.73	1123	16.0	
NGC 4303	SABbc(rs)	6.46	0.05	10.21	1620	23.1	Sey2
NGC 4314	SBa(rs)	4.17	0.05	11.22	1146	16.4	LINER
NGC 4394	SBb(r)	3.63	0.05	11.53	1036	14.8	LINER
NGC 4477	SB0(s)	3.80	0.04	11.27	1441	20.6	Sey2
NGC 4579	SABb(rs)	5.89	0.10	10.68	1607	23.0	LINER/Sey1.9
NGC 4593	SBb(rs)	3.89	0.13	11.67	2498	35.7	Sey1
NGC 4608	SB0(r)	3.24	0.08	11.96	1893	27.0	
NGC 4665	SB0/a(s)	3.80	0.08	11.50	872	12.5	
NGC 5383	SBb(rs)	3.16	0.07	12.18	2472	35.3	
NGC 5701	SB0/a(rs)	4.26	0.02	11.82	1601	22.9	LINER
NGC 5850	SBb(r)	4.26	0.06	12.04	2637	37.7	

Columns (1) and (2) give, respectively, the galaxy designation and morphological type, while column (3) shows its diameter in arcmin at the 25 B magnitude isophotal level and column (4) shows the decimal logarithm of its major to minor axes ratio at the same level. Columns (5) and (6) show, respectively, the apparent B magnitude and the radial velocity in $\mathrm{km\,s^{-1}}$. All these data were taken from RC3, except the radial velocity, taken from the Lyon Extragalactic Data Archive (LEDA), corrected for infall of the Local Group towards Virgo. Column (7) gives the distance to the galaxy in Mpc, using the radial velocity in column (6) and $H_0 = 70\,\mathrm{km\,s^{-1}\,Mpc^{-1}}$. Column (8) presents the AGN classification according to the NED.

full capabilities of the image decomposition code, i.e. its ability to model bars and AGN when necessary. Afterwards, I will show, in two separate subsections, the effects of not including these components in the models, when fitting galaxies which clearly have them.

3.1 Method and fitting functions

The code used here for the decompositions is BUDDA v2.1 (see de Souza et al. 2004). This latest version of the code has several improvements, as compared to its first version. Beside models for bulge and disc, there is now the possibility of fitting bars and a central source of light, like an AGN. The point spread function (PSF) is now described by a Moffat (1969) profile, which has been shown to reproduce the effects of atmospheric turbulence better than a Gaussian profile (Trujillo et al. 2001b). An improvement was also made to the way errors are computed for each parameter estimated by the code. The errors are estimated after the convergence of the code to the global χ^2 minimum. Each parameter is varied successively until the new χ^2 reaches a threshold equivalent to 1σ for a normal χ^2 probability distribution. This often produces meaningless error values if the parameter under consideration does not influence significantly the final χ^2 value of the model. For instance, if one has a faint disc in a lenticular galaxy, changing the disc parameters by a large amount will only produce small variations in the χ^2 of the total model. The errors obtained for the disc parameters will then be very large and meaningless. The same happens for the position angle and ellipticity of a component that is close to circular. To obtain useful error estimates, the code now weights the χ^2 threshold of each parameter by the fraction of light from the total model that comes from the component to which the parameter refers. The χ^2 threshold of the geometric parameters (position angle and ellipticity) are weighted by the ellipticity of the component. All new features in the code were tested both with synthetic and with real galaxy images. In particular, tests with artificial galaxies demonstrated that the parameters retrieved are often within 1σ of the real, input value, and almost always within 3σ. This indicates that the new procedure for error estimation gives reliable results. Nevertheless, it should be noted that these errors are purely statistical, do not take into account other sources of uncertainty, and thus must be considered as lower limits of the true error.

The disc surface brightness profile is described by an exponential function (type I disc; Freeman 1970):

$$\mu_{\rm d}(r) = \mu_0 + 1.086 r/h, \tag{1}$$

where r is the galactocentric distance, μ_0 is the disc central surface brightness and h is the disc characteristic scalelength.

The bulge surface brightness profile is described by a Sérsic function (Sérsic 1968, see Caon, Capaccioli & D'Onofrio 1993):

$$\mu_{\rm b}(r) = \mu_{\rm e} + c_n \left[\left(\frac{r}{r_{\rm e}} \right)^{1/n} - 1 \right], \tag{2}$$

where $r_{\rm e}$ is the effective radius of the bulge, i.e. the radius that contains half of its light, $\mu_{\rm e}$ is the bulge effective surface brightness, i.e. the surface brightness at $r_{\rm e}$, n is the Sérsic index, defining the shape of the profile, and $c_n = 2.5(0.868n - 0.142)$.

The AGN is modelled as an unresolved point source convolved with the PSF Moffat profile. The FWHM of the AGN profile has thus the same value of the seeing, and the only parameter fitted by the code is its peak intensity.

The bar luminosity profile is also described by a Sérsic function. For the bar,

$$\mu_{\rm Bar}(r) = \mu_{\rm e,Bar} + c_{n,\rm Bar} \left[\left(\frac{r}{r_{\rm e,Bar}} \right)^{1/n_{\rm Bar}} - 1 \right], \tag{3}$$

where $c_{n,\mathrm{Bar}} = 2.5(0.868 n_{\mathrm{Bar}} - 0.142)$, and the other parameters have similar definitions as for the bulge. Another bar parameter fitted by the code is the length of the bar semimajor axis, L_{bar}, after which the bar light profile is simply truncated and drops to zero.

Except for the AGN, which is circular, the model components are described by concentric, generalized ellipses (see Athanassoula et al. 1990):

$$\left(\frac{|x|}{a}\right)^c + \left(\frac{|y|}{b}\right)^c = 1, \quad (4)$$

where x and y are the pixel coordinates of the ellipse points, a and b are the extent of its semimajor and semiminor axes, respectively, and c is a shape parameter. Position angles and ellipticities ($\epsilon = 1 - b/a$) were fitted by the code for every component. When $c = 2$ one has a simple ellipse. When $c < 2$ the ellipse is discy, and when $c > 2$ the ellipse is boxy. For bulges and discs I fixed $c = 2$ but this parameter was left free to fit bars, since these components are better described by boxy ellipses.

Laurikainen et al. (2005) used a function to describe the bar luminosity profile which corresponds to a projected surface density of a prolate Ferrers bar (see Binney & Tremaine 1987), and showed that this results in good fits. However, they also argued that using a Sérsic function is equivalent. In fact, the Sérsic function proves to be very useful to describe the light distribution in bars. As shown by Elmegreen & Elmegreen (1985), bars in late-type spirals generally have an exponential luminosity profile, whereas bars in early-type spirals and lenticulars have a flatter luminosity profile. This duality can be conveniently expressed with the Sérsic index n: when $n \approx 1$ the Sérsic function is close to an exponential function, while for $n < 1$ one has a flatter profile. Hence, with a single function, it is possible to fit the different bar types, and quantify this difference with a single parameter. The fact that we use the same function for the luminosity profiles of bulges and bars generally does not increase the possibility of a degenerate solution. This is mainly due to two reasons. First, the geometric properties of bulges and bars in galaxy images are markedly different: bulges are rounder and centrally located while bars are more eccentric and extended. Secondly, the shape of their luminosity profiles, given by n and n_{Bar}, is in most cases also different: from the results below, one sees that n is approximately in the range of 1 to 3, whereas n_{Bar} ranges from $\approx$0.5 to $\approx$1. These differences give further constraints to find the best-fitting model for each component. Note that when the Sérsic index is below $\approx$0.15 the luminosity profile has a depression in its central parts. However, for the luminosity volume density, this occurs when the Sérsic index is below 0.5 (Trujillo et al. 2001a). We will see below that in a few cases the value found for n_{Bar} is between $\approx$0.3 and $\approx$0.5. With the uncertainties in the determination of this parameter, one cannot state firmly that these bars have outer parts more luminous that their inner parts, only based on that. Nevertheless, given the complex orbital structure of bars (see e.g. Patsis, Skokos & Athanassoula 2003), it is not very surprising to find bars with such property: it is well known that many bars do show bright structures at their ends, known as ansae, and some such structures are found in the residual images below (see e.g. Buta et al. 2006; Martinez-Valpuesta, Knapen & Buta 2007).

The initial set-up of BUDDA, where rough estimates for each parameter are given as a starting point to the code, was defined with visual inspection of the images and surface brightness radial profiles. It should be noted that, in order to achieve the best fit, the code was run several times for each image, in an interactive fashion, trying different initial set-ups, and checking the corresponding results through comparisons between the galaxy and model surface brightness profiles, the χ^2 value, estimated errors and residual images. This is particularly relevant when there is doubt about what components to include in the model. In this study, that did not happen often, but when it did it was most of the times concerning the AGN component. In these cases, the code usually shows if the component is absent in the galaxy, indicating values close to zero for its luminosity parameter. It is interesting to note that, even if a given galaxy is classified as having an AGN, this component does not necessarily need to be taken into account in a photometric model, since it can be an obscured, or a type 2, AGN, or simply not bright enough. This is in fact the case for some of the galaxies in our sample.

3.2 Results

Fig. 1 shows, for each galaxy in the sample, the original image (at two different display levels, as to emphasize either outer or inner parts), an image of the model obtained with BUDDA, and a residual image, obtained after dividing the galaxy image by the model image, both in ADU. In the residual image, brighter shades indicate regions where the model is more luminous than the galaxy, whereas darker shades indicate regions where the model is fainter than the galaxy. Fig. 1 also shows surface brightness radial profiles of the galaxy, of each component in the model separately, and of the total model, for comparison. Two sorts of brightness profile are shown. One is obtained directly from the pixel values in the corresponding images, following Laurikainen et al. (2005), and the other is obtained from ellipse fits, as usual. The results from ellipse fits also include radial profiles of position angle, ellipticity and the b_4 Fourier component. The ellipse fits were done using IRAF[1] task ELLIPSE. The surface brightness values are corrected for dust extinction in the Milky Way, and an inclination correction for intrinsic attenuation by dust was also applied (see GdS06 for further details). Fig. 1 refers to our *R*-band images but similar results were found in the *V* band. The values of the relevant structural parameters obtained are displayed in Tables 2 and 3 for both bands. Note that the disc parameters obtained for NGC 4151, 4665 and 5850 suffer from large uncertainties due to their intrinsic low surface brightness and the issues on sky subtraction mentioned above.

From Fig. 1 it is possible to verify that the models obtained are a fairly good representation of their corresponding galaxies, checking either the images provided or the radial profiles. Inspecting the residual images, it is possible to identify many substructures, such as spiral arms (e.g. NGC 4394), inner discs (e.g. NGC 4151), inner spirals (e.g. NGC 4314), nuclear rings (e.g. NGC 4593), inner bars (NGC 5850), ansae at the ends of the bar (e.g. NGC 4151, 4608 and 5850), dust lanes (e.g. NGC 4303 and 5383) or more complex dust structure (e.g. NGC 2110 and 2911). Although some such structures can be seen in the original galaxy images, in all cases they stand out much more clearly in the residual images. This confirms residual images as a powerful tool to study these galactic components. It is worth noting that, for many of our barred galaxies (but not all), the residual images reveal a very elongated structure, inside the bar, along its major axis. This confirms the theoretical study of Athanassoula (1992), where the morphology of orbits in barred galaxies is analysed. She found that, close to the major axis of the bar, the dominant family of orbits is indeed very elongated, and that the orbits become less eccentric away from the major axis (see her

[1] IRAF is distributed by the National Optical Astronomy Observatories, which are operated by the Association of Universities for Research in Astronomy, Inc., under cooperative agreement with the National Science Foundation.

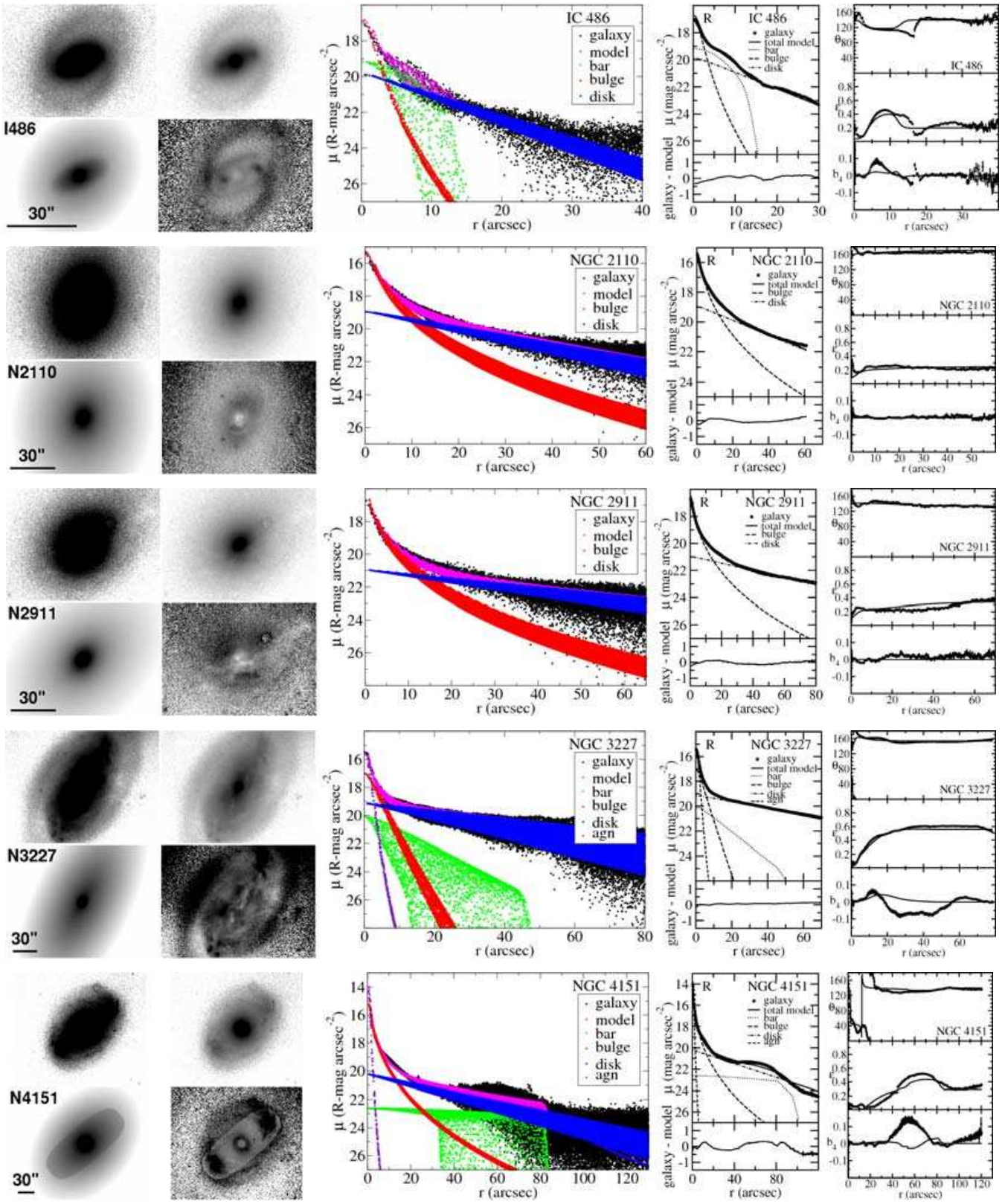

Figure 1. Results of image decomposition in the *R* band for each galaxy in the sample. The images on the left show the galaxy with emphasis on its outer (top left) and inner parts (top right), as well as the model and residual images (bottom left and right, respectively). In the latter, brighter shades indicate regions where the model is more luminous than the galaxy, whereas darker shades indicate regions where the model is fainter than the galaxy. The panel at the centre shows the surface brightness profiles of the galaxy and the models as indicated. Each point in these profiles corresponds to a single pixel. Only 10 per cent of the pixels are shown. The panels on the right show the results of ellipse fits to the galaxy and model images. These are radial profiles of surface brightness (elliptically averaged) with residuals, and geometric parameters: position angle (from north to east – top), ellipticity (centre) and the b_4 Fourier coefficient (bottom).

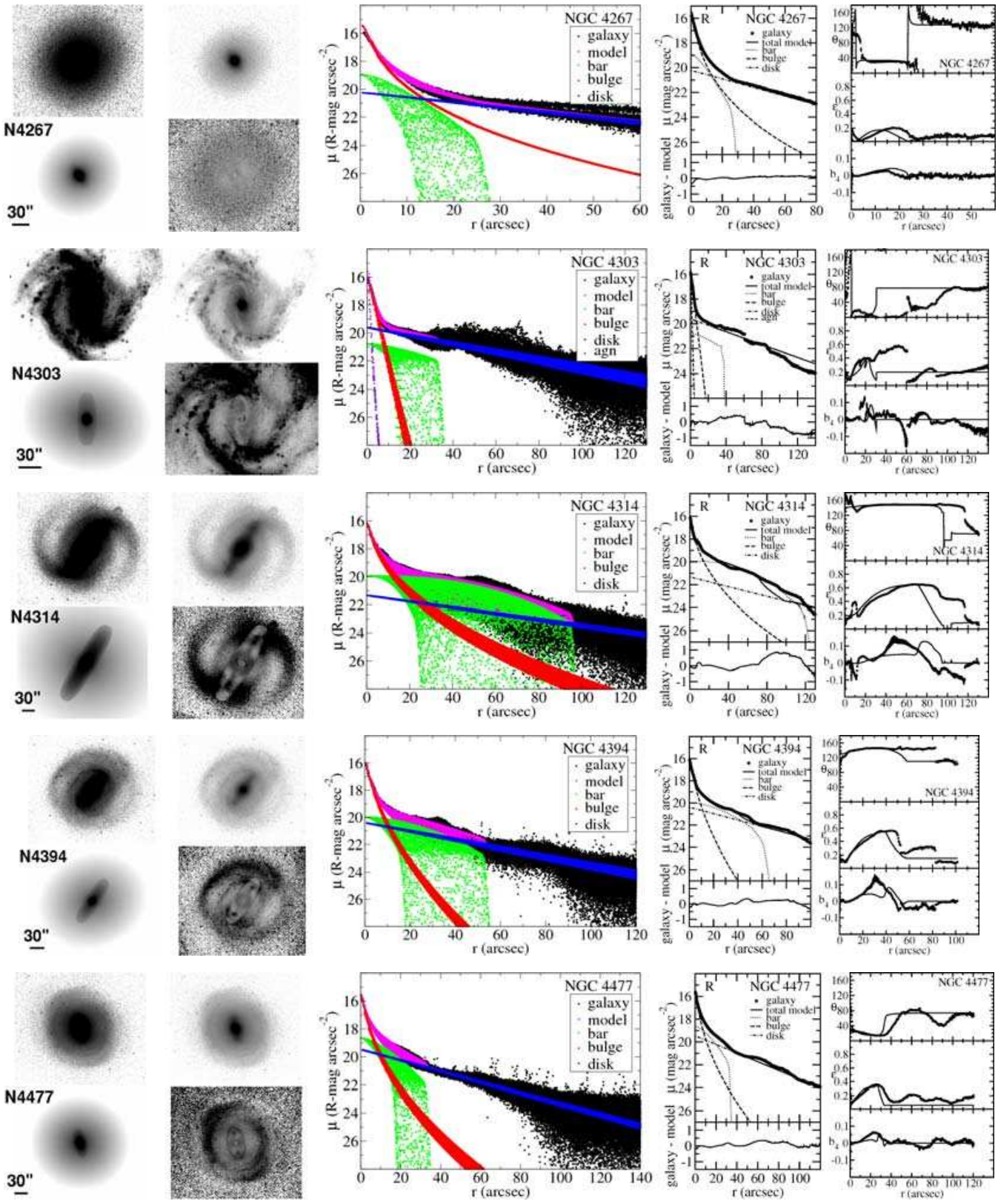

Figure 1 – *continued*

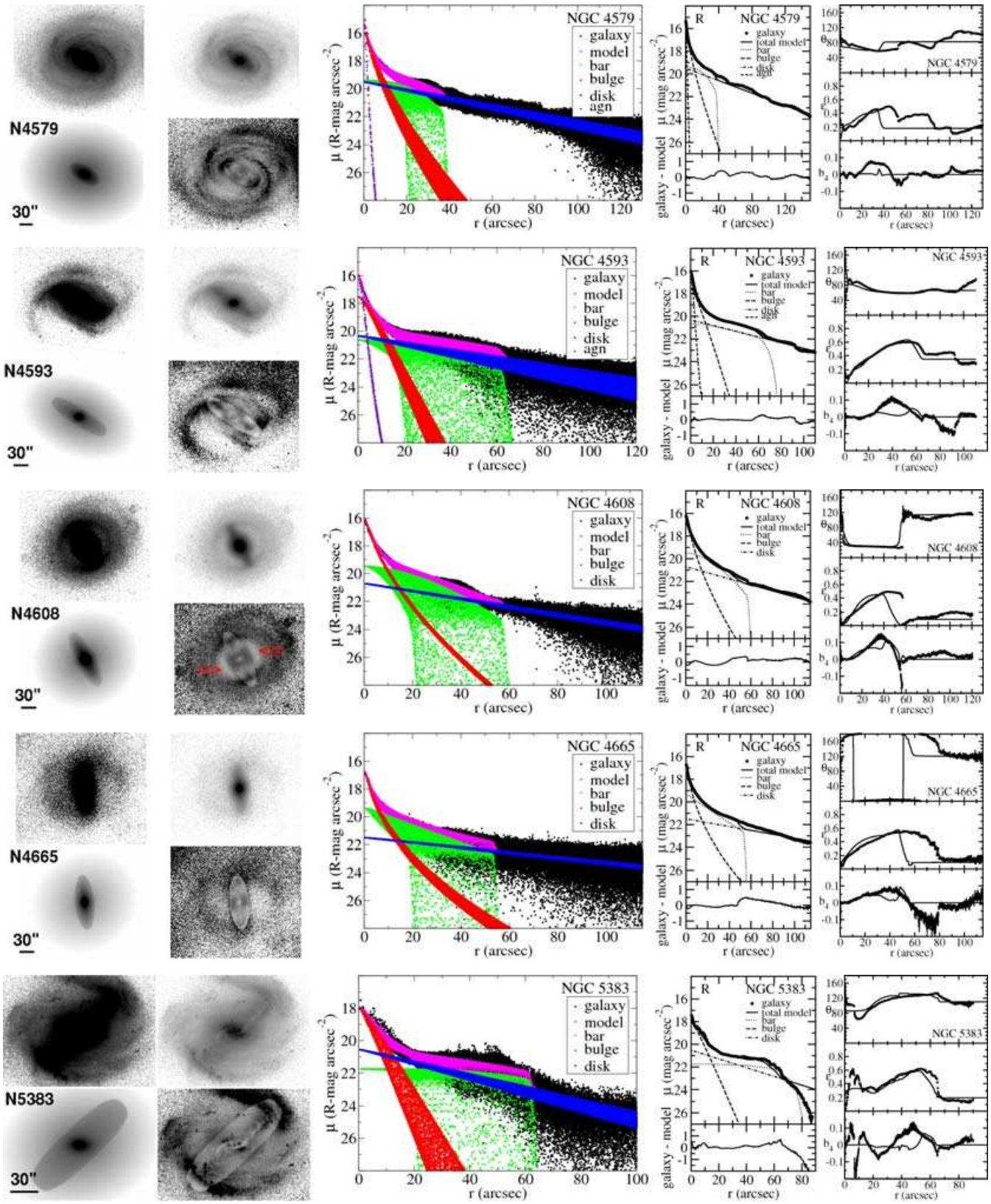

Figure 1 – *continued*

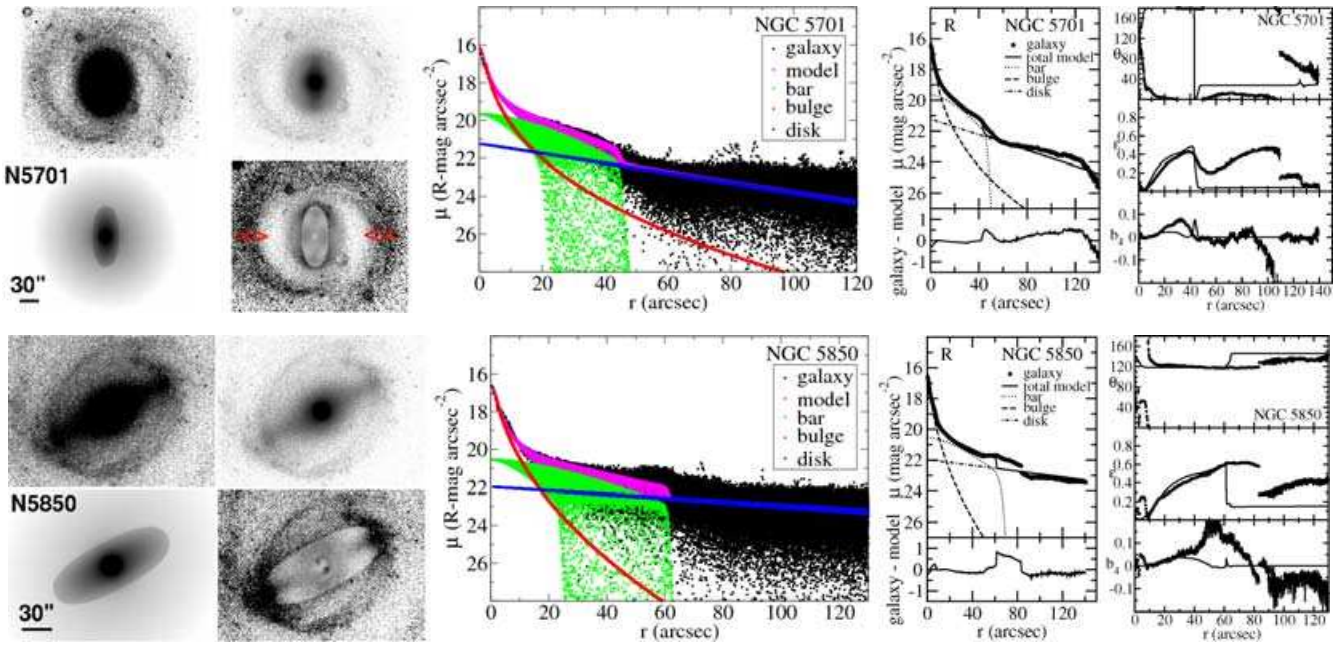

Figure 1 – *continued*

Table 2. Galaxy structural parameters in the *R* band.

Galaxy	μ_0	h	μ_e	r_e	n	n_{Bar}	L_{Bar}	ϵ_{Bar}	c	B/T	D/T	Bar/T
(1)	(2)	(3)	(4)	(5)	(6)	(7)	(8)	(9)	(10)	(11)	(12)	(13)
IC 486	19.7	8.9	17.6	1.1	2.1	0.49	12.7	0.54	2.12	0.213	0.579	0.208
NGC 2110	18.9	21.8	18.2	6.8	2.7					0.390	0.610	
NGC 2911	20.9	41.0	19.6	7.1	3.0					0.354	0.646	
NGC 3227	19.1	38.3	18.2	3.7	1.1	1.00	45.8	0.74	2.80	0.068	0.876	0.017
NGC 4151*	20.2	33.7	18.0	4.7	3.0	0.60	82.1	0.60	3.07	0.327	0.503	0.082
NGC 4267	20.2	31.1	18.2	4.8	3.1	0.77	25.5	0.60	2.42	0.356	0.593	0.051
NGC 4303	19.6	41.7	17.6	3.0	1.0	0.67	33.3	0.65	2.80	0.066	0.898	0.028
NGC 4314	21.3	53.0	19.2	10.2	2.2	0.40	95.4	0.75	2.89	0.296	0.397	0.308
NGC 4394	20.4	37.4	18.2	4.2	1.8	0.56	53.1	0.70	2.76	0.186	0.676	0.138
NGC 4477	19.5	28.7	18.0	5.0	2.0	0.66	32.9	0.50	1.96	0.183	0.689	0.128
NGC 4579	19.5	39.5	17.9	5.2	1.4	0.38	37.5	0.50	2.04	0.127	0.749	0.115
NGC 4593	20.3	43.0	18.7	6.5	0.9	0.66	62.2	0.73	2.72	0.157	0.671	0.127
NGC 4608-I	20.7	40.7	18.3	5.2	1.7	0.58	57.6	0.66	2.02	0.257	0.565	0.178
NGC 4608-II	20.2	33.4	18.7	6.9	2.1	0.58	57.6	0.66	2.02	0.327	0.491	0.182
NGC 4665*	21.5	63.6	19.4	5.9	2.0	1.06	54.0	0.65	1.99	0.152	0.676	0.172
NGC 5383	20.5	28.1	19.5	7.0	0.9	0.31	62.0	0.69	2.96	0.166	0.651	0.183
NGC 5701	21.2	42.9	19.2	6.5	3.2	0.62	44.7	0.56	2.35	0.278	0.501	0.221
NGC 5850*	22.0	116.6	19.0	5.3	2.1	0.64	60.9	0.61	2.44	0.172	0.681	0.147

Structural parameters of bulges, discs and bars. Column (1) gives the galaxy name, while columns (2) and (3) show, respectively, the disc central surface brightness and scalelength. Columns (4), (5) and (6) show the bulge effective surface brightness, effective radius and Sérsic index, respectively. Columns (7) and (8) show the Sérsic index of the bar luminosity profile and the length of the bar semimajor axis, respectively. Column (9) shows the bar ellipticity, whereas column (10) shows the shape index of the bar isophotes. Finally, columns (11), (12) and (13) give, respectively, the estimated luminosity fractions of bulge, disc and bar. Luminosity parameters are in units of mag arcsec^{-2} and scalelengths in arcsec. Galaxies marked with * have uncertain estimates for the disc parameters. The two rows for NGC 4608 correspond to the fits with a type I and a type II disc, as indicated.

fig. 12). It seems that the ellipsoid that fits the bar is able to account for the external, less eccentric orbits, which are spread over most of the bar, but the very elongated inner orbits show up in the residuals. It is plausible that a model for the bar with an ellipticity that varies radially could fit most of the orbits. Alternatively, one could use two ellipsoids for the bar: one as used here, and another, much more eccentric, but this is beyond the scope of this study. It is also interesting to note that the same residual images show another structure within the bar, but this is only in the central region of the galaxy. This could be associated with an inner disc or a lens.

As mentioned, two types of surface brightness profile are shown. The one derived pixel-by-pixel has the advantage of displaying information from the image as a whole, which is hidden in the elliptically averaged profile from ellipse fits. The spread of the points in each pixel-by-pixel profile indicates (i) in the models, the geometry of the corresponding model component (circular components

Table 3. Galaxy structural parameters in the *V* band.

Galaxy (1)	μ_0 (2)	h (3)	μ_e (4)	r_e (5)	n (6)	n_{Bar} (7)	L_{Bar} (8)	ϵ_{Bar} (9)	c (10)	B/T (11)	D/T (12)	Bar/T (13)
IC 486	20.1	8.3	18.0	1.1	2.7	0.47	12.6	0.57	2.24	0.239	0.562	0.199
NGC 2110	18.8	17.0	18.6	6.1	3.4					0.348	0.652	
NGC 2911	21.4	32.7	20.2	7.0	2.6					0.389	0.611	
NGC 3227	19.5	39.9	19.2	4.5	0.6	1.00	45.8	0.74	2.80	0.049	0.905	0.007
NGC 4151*	20.6	33.7	18.2	4.2	3.8	0.60	82.1	0.60	3.07	0.361	0.481	0.082
NGC 4267	21.0	33.6	18.8	5.3	3.4	0.77	22.3	0.60	2.42	0.396	0.557	0.048
NGC 4303	20.1	43.7	18.2	3.1	1.0	0.67	33.3	0.65	2.80	0.061	0.904	0.024
NGC 4314	22.0	58.4	19.8	10.9	2.0	0.37	95.7	0.75	2.89	0.304	0.395	0.301
NGC 4394	20.8	37.0	18.7	4.2	1.9	0.60	53.0	0.71	2.76	0.184	0.685	0.131
NGC 4477	19.9	27.5	18.6	4.9	1.8	0.71	32.9	0.50	2.05	0.168	0.695	0.137
NGC 4579	19.9	38.3	18.4	5.4	1.2	0.29	38.5	0.52	1.96	0.125	0.754	0.109
NGC 4593	20.7	46.2	19.3	6.9	0.7	0.63	62.2	0.73	2.67	0.133	0.710	0.112
NGC 4608	21.5	46.8	18.9	5.5	1.9	0.63	57.8	0.63	2.02	0.268	0.540	0.192
NGC 4665*	20.7	48.7	19.2	6.4	2.1	1.06	54.0	0.65	1.99	0.149	0.687	0.164
NGC 5383	21.0	30.5	19.9	7.1	0.8	0.38	62.0	0.70	2.89	0.147	0.698	0.155
NGC 5701	22.0	63.2	19.9	7.0	3.2	0.62	45.6	0.56	2.35	0.240	0.567	0.193
NGC 5850*	22.4	118.9	19.5	5.1	2.0	0.58	60.9	0.62	1.99	0.152	0.719	0.130

Structural parameters of bulges, discs and bars. As in Table 1 but from the *V*-band images. Luminosity parameters are in units of mag arcsec^{-2} and scalelengths in arcsec. Galaxies marked with * have uncertain estimates for the disc parameters.

have very narrow profiles), and (ii) in the galaxies, their geometrical properties and the deviation from the average of the light distribution through the galaxy surface due to its own features (e.g. spiral arms, dust, star-forming regions) and statistical fluctuations in the photometry. None the less, the usual ellipse fit profile is shown for the sake of comparison. From these profiles, one sees models that range from excellent fits (e.g. NGC 2911, 3227 and 4267), corresponding usually to more simple galaxies, to fits where residuals are significant (e.g. NGC 4303, 4314 and 5850), usually galaxies with bright spiral arms and complex structure. Nevertheless, a typical difference between galaxy and model is about only ± 0.25 mag arcsec^{-2}. It is interesting to note that, while bulges and discs dominate the inner and outer parts of galaxies, respectively, bars can be the dominant structure at intermediate radii (see IC 486, NGC 4314, 4608, 4665, 5701 and 5850).

Interestingly enough, from the ellipticity and position angle profiles in Fig. 1, one sees that only by including a bar it is possible to fit the rise and drop in ellipticity and the abrupt changes seen in position angle, both features typical of barred galaxies (see e.g. NGC 4151, 4267 and 4608). The remaining discrepancies in the position angle and ellipticity profiles seem to be caused by other components, such as spiral arms, rings and ovals (see Gadotti et al. 2007), present in the galaxy but not in the models. For instance, this is clear in NGC 4303, 4314, 4394 and 5701. In the models, after the bar end, usually accompanied by a sudden change in position angle and a drop in ellipticity, these parameters assume the values of the disc component. In the galaxies, however, if there is an additional component between the bar and the outer disc, with position angle and ellipticity different from those of the disc, then there will be differences between the corresponding galaxy and model radial profiles. The radial profiles of b_4 are the ones with strongest disagreement between galaxies and models. Either the models do not reproduce the position where the peak in b_4 happens, or the corresponding b_4 values. There is no clear reason why these discrepancies occur. Nevertheless, NGC 3227, 4151 and 5850, where these disagreements are particularly severe, show either conspicuous dust structure or very bright ansae at the end of the bar.

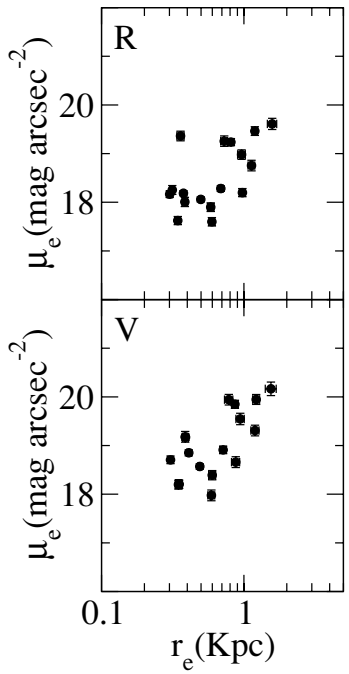

Figure 2. Correlation between the effective surface brightness and the effective radius of bulges, for the galaxies in the sample, in both bands.

It is interesting to verify if known results can be reproduced with the output from the decompositions shown here. Fig. 2 shows the correlation between the effective surface brightness and the effective radius of bulges, for the galaxies in the sample, in both bands. This correlation was first found by Kormendy (1977) for elliptical galaxies and afterwards shown to hold also for bulges. A similar correlation was found between the central surface brightness and the scalelength of discs (see e.g. de Jong 1996). Fig. 3 shows that this correlation is reproduced when one considers our *V*-band

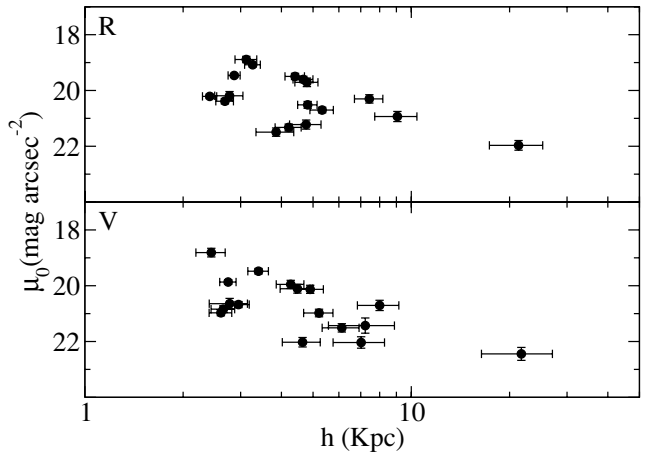

Figure 3. The central surface brightness of discs plotted against their scalelengths, for the galaxies in the sample, in both bands, as indicated.

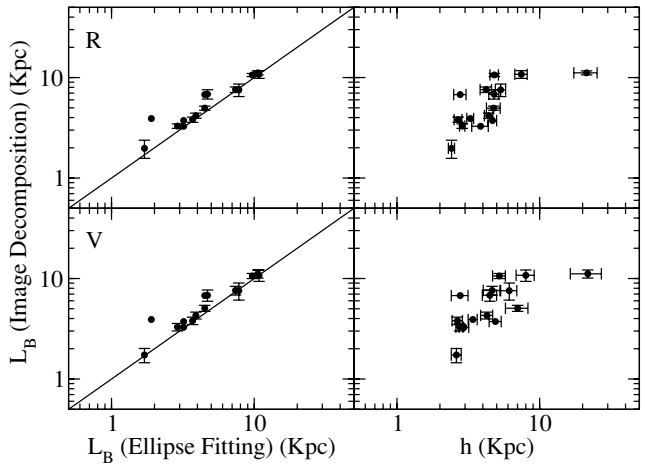

Figure 4. Left: correlation between the length of bars from image fitting and from the measurements using ellipse fits in GdS06. The solid lines depict a perfect correspondence. Right: correlation between the length of bars from image fitting and the scalelength of discs. The outlying point corresponds to NGC 5850, whose disc parameters suffer from large uncertainties. These results include all barred galaxies in the sample, in both bands, as indicated.

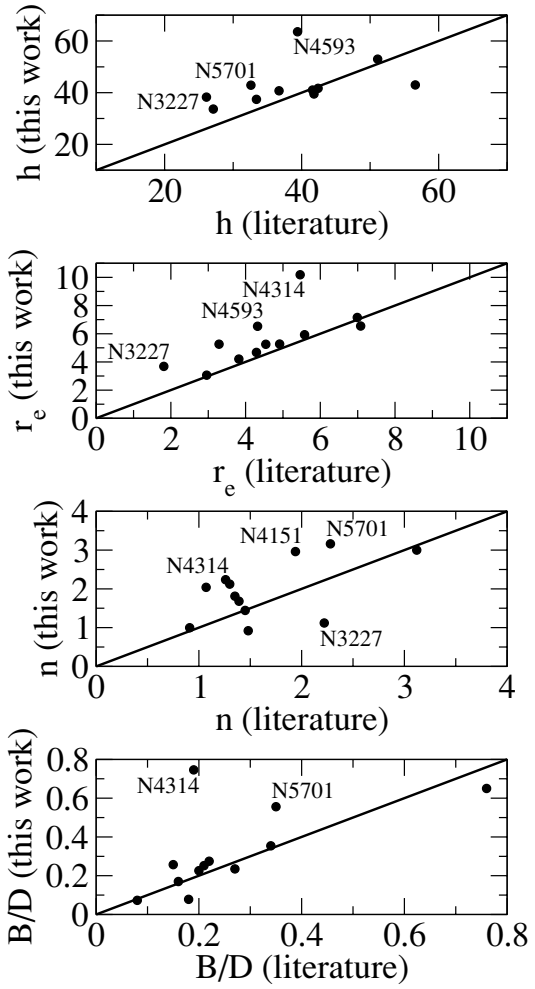

Figure 5. Comparison between some structural parameters obtained in this work with those found in Laurikainen et al. (2004, 2005) for the same galaxies. From top to bottom: disc scalelength, bulge effective radius, bulge Sérsic index and bulge-to-disc luminosity ratio. Scalelengths are in arcsec. Some cases where a good agreement was not found are indicated. The solid lines depict a perfect correspondence.

images, albeit with a large scatter. The scatter is even larger when one looks at the results from our *R*-band images, rendering the correlation not significant in this case, in particular if one ignores the outlying point, which corresponds to NGC 5850, whose disc parameters suffer from large uncertainties. However, it is reasonable to assume that this is mostly a statistical effect, as the sample is not particularly large, and thus that the correlation is real. The length of bars is also correlated with the disc scalelength, as shown in Fig. 4 and by e.g. Erwin (2005). This figure also shows that the bar lengths estimated with BUDDA agree very well with the estimates from ellipse fits in GdS06. This is not surprising, since the latter are used as a starting point for the code, but it is interesting to find such a good agreement as this parameter was not kept fixed in the fits.

3.3 Comparison with previous fits

Fig. 5 shows a comparison between some structural parameters obtained in this work with those found in Laurikainen et al. (2004, 2005) for 12 galaxies also studied by them. In these papers, the structural parameters are also obtained via an image decomposition code, able to fit bulges, discs and bars. The main methodological differences between this study and theirs are (i) they used a Ferrers model to describe the bar luminosity profile, (ii) they fitted an additional component (an oval) in NGC 4608, (iii) they have not modelled the AGN light contribution and (iv) they used near-IR images. Fig. 5 shows that there is generally good agreement between our measurements. For 10 of the 12 galaxies, they have fixed the bar model to a very flat luminosity profile, but it seems that the use of a different bar model does not lead to significantly different results. The modelling of the oval in NGC 4608 also did not produce a fit significantly different from the one shown here. However, I will show below that a better fit to this particular galaxy can be achieved using a Freeman type II disc (Freeman 1970), rather than a type I. Nevertheless, for some galaxies, the values of some structural parameters obtained here and by Laurikainen et al. are discrepant. Most of these cases are pointed out in the figure. As already mentioned, the fit to NGC 4151 is dubious. Likewise, Laurikainen et al. state that their results to NGC 3227, 4151 and 5701 can also

be compromised: the authors mention that their images are not deep enough and the resulting parameters are uncertain. Since their images are in the near-IR and ours in the optical, and given that galaxies usually become bluer outwards (but see Gadotti & dos Anjos 2001), the scalelengths obtained here could indeed be somewhat larger than theirs. This systematic difference seems to be present in Fig. 5 but complicates these comparisons. This difference in wavelength could also explain the different results for NGC 3227, 4314 and 4593, which have significant amounts of dust and star formation which certainly have a stronger effect in the optical than in the near-IR. In particular, NGC 4314 has very bright star-forming nuclear spiral arms that show up clearly in the residual image. The light from these spirals is partially attributed to the bulge component, and, since these spirals should not be so conspicuous in the near-IR, this can explain why I obtain a much more massive bulge than Laurikainen et al. On the other hand, it is not clear why our results are discrepant for the bulge of NGC 5701, although the difference in the Sérsic index is within typical 1σ errors. Furthermore, it is unclear if the AGN light should have been taken into account also in their near-IR images. Taken altogether, this general agreement, and the fact that with the results presented here it is possible to reproduce some known results (Figs 2, 3 and 4) are very encouraging.

3.4 The ellipticity of bars

To measure the ellipticity of a bar, one usually fits ellipses to the galaxy image and assumes that the bar ellipticity is that of the most eccentric fitted ellipse (e.g. Marinova & Jogee 2007). This is a very important parameter because it is strongly related with the strength of the bar, and can provide constraints for bar models, like those of e.g. Athanassoula & Misiriotis (2002) and secular evolution scenarios (e.g. Gadotti & dos Anjos 2001). In Fig. 6, the ellipticity of bars as estimated from the image decompositions are plotted against the ellipticity peak in the ellipse fits of GdS06. The latter is used as a starting point for the decompositions but the bar ellipticity is a free parameter in the fits. It is clear that ellipse fits underestimate the true ellipticity of the bar. This effect is on average about 20 per cent, but it can be as large as a factor of 3. For NGC 5850, however, the match between the two parameters is excellent. Examining the cases where this effect is strongest, as in NGC 4267 and 4303, reveals its origin: the ellipticity of the isophotes in the bar region is diluted by the contribution from the round, axisymmetric component of the galaxy. The strength of this effect is thus governed by the difference between the contributions of the bar and the disc to the total light in the galaxy near the bar end, since it is about this region where the bar isophotes reach their peak in ellipticity, and the bulge component is usually faint there. As the disc of NGC 5850 is very faint, this dilution is not efficient in this galaxy.

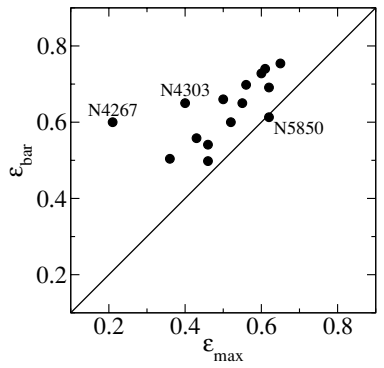

Figure 6. Ellipticity of bars estimated from image decomposition plotted against the ellipticity peak in ellipse fits from GdS06. Some interesting cases are indicated. The solid line indicates a perfect correspondence. It is clear that ellipse fits systematically underestimate the true ellipticity of the bar.

These results have implications on previous findings in the literature. For instance, Marinova & Jogee (2007) measured the bar ellipticity via ellipse fits in a sample of 180 barred galaxies. They found that only a minority of the bars in their sample have ellipticities below 0.4, and that most bars have ellipticities between 0.5 and 0.8, with a mean value of about 0.5. As I have just shown, ellipse fits systematically underestimate the true bar ellipticity by 20 per cent, on average. This means that the paucity of weak bars, i.e. those with ellipticities below 0.4, is even more pronounced. Many of these bars in their sample might have higher ellipticities, which, however, cannot be reliably measured with ellipse fits due to the effects just discussed. Furthermore, the fraction of bars with high ellipticities is, in fact, even higher, as is the true mean value for the ellipticity of bars. A simple calculation gives a true mean value of around 0.6, considering an underestimation of 20 per cent.

It should be noted that the bar strength does not depend only on the bar ellipticity, but also on its shape (more rectangular, boxy bars, i.e. those with higher c, are stronger) and its mass (see also discussion in Marinova & Jogee 2007, and references therein). The strength of a bar is thus directly connected to the amplitude of the non-axisymmetric potential it introduces in the overall potential well of its host galaxy. With this definition, the strength of a bar does not depend on any other of the properties of its host galaxy. On the other hand, the impact of a bar on the evolution of a galaxy depends on other galaxy properties. A strong bar will significantly modify the dynamics of gas and stars in a galaxy with a relatively weak axisymmetric potential, i.e. a galaxy where the bar mass is high compared to the bulge and disc masses. The same bar would produce less significant effects in a galaxy with massive bulge and disc. Furthermore, since the axisymmetric component of the potential is centrally concentrated, mainly due to the bulge, the changes due to the bar are likely to have a dependence on radius and to be more significant closer to the bar ends.

3.5 Disc consumption in NGC 4608 and 5701

It is not uncommon to see in residual images such as those in Fig. 1 regions with evident negative residuals, where the fitted model is brighter than the galaxy. In some cases, this is clearly a result of dust extinction, but in other cases their presence might mean that the models used are not fully adequate. Inspecting the results in Fig. 1, it is possible to identify two particular cases where such negative residuals are not only conspicuous, but also clearly delineate a distinct region in the residual image. These are NGC 4608 and 5701. In their residual images, one is able to spot a region in the disc where the models are definitely brighter than the galaxies. It can be described as two crescents, one at each side of the bar, but out of it (pointed out by the red arrows in Fig. 1). In NGC 4608, these crescents extend to a radius similar to the bar semimajor axis length, i.e. up to the inner ring surrounding the bar. In NGC 5701, this region is more extended, and the crescents occupy the whole area between the bar and the outer ring. In Gadotti & de Souza (2003), this less luminous area in the disc component of these galaxies was identified, and it was pointed out that the *N*-body models of bar formation and evolution presented in Athanassoula & Misiriotis (2002) produce a very similar feature, particularly their models which lead to the formation of very strong bars (see their fig. 3). Athanassoula (2002, 2003) presents theoretical work which shows that bars get longer

with age by capturing disc stars, which is in agreement with the observational findings in Gadotti & de Souza (2005) and GdS06, although more observational evidences are needed to settle this point. Thus, these fainter areas in the discs of NGC 4608 and 5701 are plausibly created by such capture of stars. If this is indeed the case, then these galaxies provide an excellent opportunity to gather insight on these theoretical results and the secular evolutionary processes in barred galaxies. One of the implications from these studies is that the initially exponential density profile of a stellar disc in a given galaxy would evolve into a more complex structure, which can be better described by a density profile which is flatter in the inner part, as compared to the outer part. Such a profile is reminiscent of a Freeman type II profile (Freeman 1970), which is exponential in the outer part and flatter in the inner part. The amount of flattening in the inner part of the disc profile of both NGC 4608 and 5701 can then give us a quantitative measure of these secular evolution processes.

An issue in the results presented in Gadotti & de Souza (2003) was that the model used to fit these galaxies did not include a bar. In fact, the absence of this component disturbed the fit to the extent that it was not possible to find a solution for the disc component of both NGC 4608 and 5701. Laurikainen et al. (2005) investigated this issue in both galaxies and, using a model that includes a bar, found similar results as the ones shown in Fig. 1. After accounting for the bar, a solution for the disc is possible, but the negative residuals in the inner disc still remain significant.

In order to obtain a better fit to NGC 4608, i.e. one in which the match between model and galaxy is better in the inner, fainter part of the disc, and thus does not produce such strong negative residuals, and at the same time be able to quantify how faint the inner part of the disc is compared to what would be expected from a single exponential profile for the whole disc, I tried another two models for the disc component. In both models, the disc luminosity profile is exponential, as before, but only from a certain radius outwards. The difference resides in the behaviour of the profile from this point inwards: in the first model, the profile is abruptly truncated, it falls to zero, and so the disc has a hole in the centre; in the second model, the profile stops rising exponentially and is kept at a constant value all the way to the centre, so that the disc is similar to a Freeman type II disc (note that this model has a much stronger physical justification than the former). The fitting in these cases was done keeping the bar component as found in the best fit using a type I disc. The radius at which the disc profile changes is left as a free parameter. The top panel in Fig. 7 compares the three models. It shows radial profiles built from the residual images along a stripe perpendicular to the bar, and with a width of 5 pixel, from which an average value was taken using both sides from the centre at each galactocentric radius. Since the residual images are built dividing the galaxy image by the model image, values above one in these profiles indicate that the galaxy is brighter than the model at the corresponding pixels, whereas values below one indicate that the model is brighter. The fainter, inner part of the disc in NGC 4608 can easily be identified in this figure, as a depression between $r \approx 20$ and 50 arcsec. One sees that, at the minimum of this depression, the model with a normal, type I disc is almost a factor of 2 brighter than the actual disc. On the other hand, using the model with a hole in the disc does not result in a better fit, since in this case one sees now a significant positive residual between $r \approx 20$ arcsec and the truncation radius. In the fit with a type II disc, however, the match between model and galaxy is clearly improved. The full results of this fit are shown in Fig. 8 and also in Table 2. The better agreement is evident in the residual image, in the residuals of the elliptically averaged brightness profiles, and

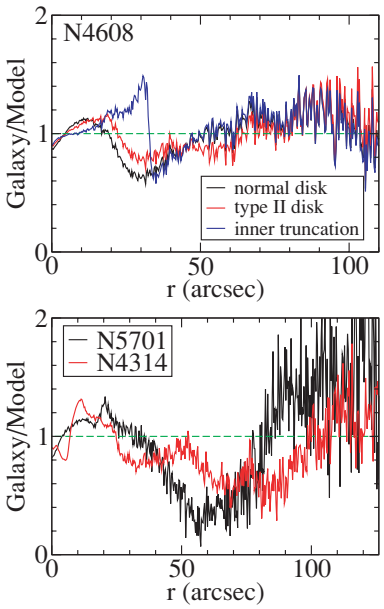

Figure 7. Radial profiles of the residuals from the three different models for NGC 4608 (top panel) and from the models for NGC 5701 and 4314 (bottom panel). These profiles were built with the residual images along a stripe perpendicular to the bar, and with a width of 5 pixel, from which an average value was taken using both sides from the centre at each galactocentric radius. One sees that the best-fitting model for NGC 4608 is the one where the disc is a type II disc (see also Fig. 8), rather than the usual disc, that goes exponentially all the way to the centre (type I), or the disc with an abrupt inner truncation. In addition, the area of the disc in NGC 5701 between the bar and the outer ring is about two–three times fainter than the model. As a comparison, on can also see negative residuals in the disc between the bar and the spiral arms in NGC 4314, but it is a less pronounced effect. In all the other galaxies in the sample such negative residuals are not conspicuous.

also in the ellipticity profile, where the steep drop at the end of the bar is now better reproduced. As expected, the value found by the code for the radius of the break in the disc profile is similar to the bar length (55 arcsec, i.e. ≈2 arcsec less than $L_{\rm Bar}$). Note that the brightness profile of the galaxy also has a break at this point. Furthermore, there is an improvement of ≈25 per cent in the χ^2 value. Interestingly, the disc luminosity fraction falls from 0.565 (using a type I disc model) to 0.491 (with a type II disc), i.e. 7.4 per cent of the total galaxy luminosity, which is ≈40 per cent of the bar luminosity. Assuming that NGC 4608 had a type I disc initially, and that the stars from the inner disc migrated to the bar, resulting in the change of the disc profile to a type II, then one can conclude that the bar increased in mass by a factor of ≈1.7, through the capture of ≈13 per cent of the disc stars. This assumes the same mass-to-light ratio in the bar and in the disc, but is reasonable enough for an order of magnitude estimation. In fact, we showed in GdS06 that the $B - R$ colours of the bulge, disc and bar in NGC 4608 are very similar, meaning that the corresponding mass-to-light ratios might not be too different.

For NGC 5701 it was not possible to obtain an alternative fit. When trying both the inner truncated disc and the type II disc, the radius at which the disc profile changes, as found by the code, is close to the centre, and thus the resulting model is not significantly different from the previous one. A possible explanation for this difference is that in NGC 4608 the two crescents together form a well defined single region with negative residuals, whereas in NGC 5701

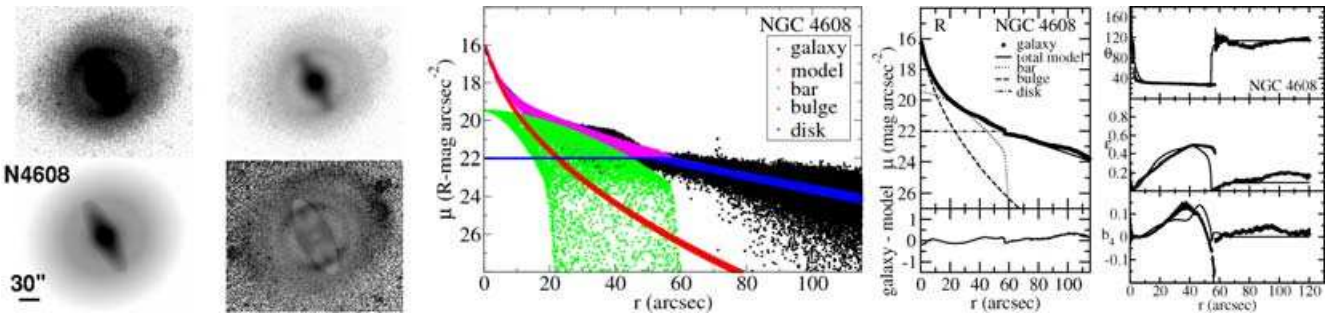

Figure 8. Similar to Fig. 1, but when the disc in NGC 4608 is modelled as a Freeman type II disc. Comparing the results obtained from both models it is clear that a type II disc produces a better fit to this galaxy.

the two crescents are more detached from each other, resulting in two separate regions with negative residuals. Thus, it seems that a more complex model is necessary. In Figs 1 and 7 one sees that the mismatch between galaxy and model in the inner disc of this galaxy is even more accentuated than in the case of NGC 4608. The area of the disc in NGC 5701 between the bar and the outer ring is about two–three times fainter than the model. In almost all the other galaxies in the sample such negative residuals are not conspicuous, the only exception being NGC 4314. Figs 1 and 7 show, however, that this effect is less pronounced in this galaxy.

3.6 The effects of neglecting bars

In order to study the effects of not modelling bars on the structural parameters obtained from image decomposition, the fitting of the barred galaxies in the sample was repeated with the bar removed from the models. As I will shortly show, bulge models are significantly altered when bars are not taken into account, to accommodate the light from the bar. Thus, in this exercise, I fixed the ellipticity and position angle of the bulge, with the results found in Section 3.2, minimizing the distortion in the bulge models. This means that the effects caused by ignoring bars, as found here, are actually lower limits. Apart from these differences, the fitting process was identical to that of the main fits. This exercise was done only with the *R*-band images, and excludes the five galaxies in the sample for which the AGN contribution has to be modelled, to avoid complicating the interpretation of the results.

Fig. 9 compares the structural parameters of discs and bulges, and the disc-to-total and bulge-to-total luminosity ratios, as estimated when bars are not included in the models, with the same parameters when bars are taken into account. It is clear that both bulge and disc components are altered in order to accommodate the light from the bar. Discs tend to assume a steeper luminosity profile, meaning brighter μ_0 and shorter h. As a consequence, the disc luminosity fraction increases. A stronger effect is seen in the bulges, which get bigger to account for the bar, acquiring larger r_e and luminosity fractions. The changes in μ_e and n are within the uncertainties but it seems to be a systematic effect towards fainter μ_e and smaller n. It is interesting to note that in some cases there was no significant change. Evidently, if the bar contributes to a large fraction of the total galaxy luminosity these effects will be more pronounced. None the less, other features in the galaxy might have a relevant role as well. For instance, if the geometrical parameters of the bar are very different from those of both bulge and disc, this will give further constraints to help the code in order to separate the different components, even if the bar is not modelled. To evaluate the exact circumstances that aggravate this issue is beyond the scope of this study. The relevant points to stress here are the presence of systematic effects at play when bars are not considered in the models, and the fact that these effects alter primarily the structural parameters obtained for bulges. Fig. 9 shows that the disc luminosity fraction is overestimated, on average, by 10 per cent, with a maximum overestimation of 30 per cent. The bulge luminosity fraction is overestimated, on average, by 50 per cent, and this overestimation can be as high as a factor of 2.

Fig. 10 illustrates the effects of not including the bar in the fitted model in a more detailed fashion, for an individual case, that of IC 486. This figure should be compared with Fig. 1, which shows the results from a fit that includes a bar component in the model. One sees that the disc acquires a steeper profile (h gets shorter by about 25 per cent), with a brighter central surface brightness (0.73 mag brighter), while the effective radius of the bulge grows about 25 per cent. The disc luminosity fraction increases 20 per cent, whereas the bulge luminosity fraction increases 45 per cent. These changes are reflected in the residual image: the bulge model absorbs the inner part of the bar, and the brightened bulge and disc models produce strong negative residuals.

3.7 The effects of neglecting bright AGN

For five galaxies in the sample it was deemed necessary to include the AGN component in the model in order to obtain proper fits. To study the effects of not modelling the AGN on the structural parameters obtained from image decomposition, the fitting of these galaxies was repeated with the AGN component removed from the models. Again, apart from that, the fitting process was identical to that of the main fits, and only *R*-band images were used.

Fig. 11 compares the structural parameters of bulges, and the bulge-to-total luminosity ratio, as estimated when AGN are not accounted for in the models with the same parameters when AGN are taken into account. The disc and bar components are not significantly affected when ignoring the AGN contribution. The figure shows that, due to the concentrated light from the AGN, if it is not taken into account, bulges tend to become smaller and more luminous, i.e. with shorter effective radius and brighter effective surface brightness. Most importantly, the Sérsic index of the bulge is severely affected, being overestimated by up to a factor of 4. As a result of these changes, the bulge luminosity fraction is also overestimated, up to factor of 2. For two of these galaxies, NGC 4303 and 4579, where the AGN component corresponds to only ≈1 per cent of the total galaxy light, these effects are small. For the remaining three, NGC 3227, 4151 and 4593, where the AGN luminosity fraction ranges from ≈4 to ≈9 per cent, these effects are significant. In addition, although the number of points is small, these changes seem to be systematic. Thus, it is clear that the bulge parameters

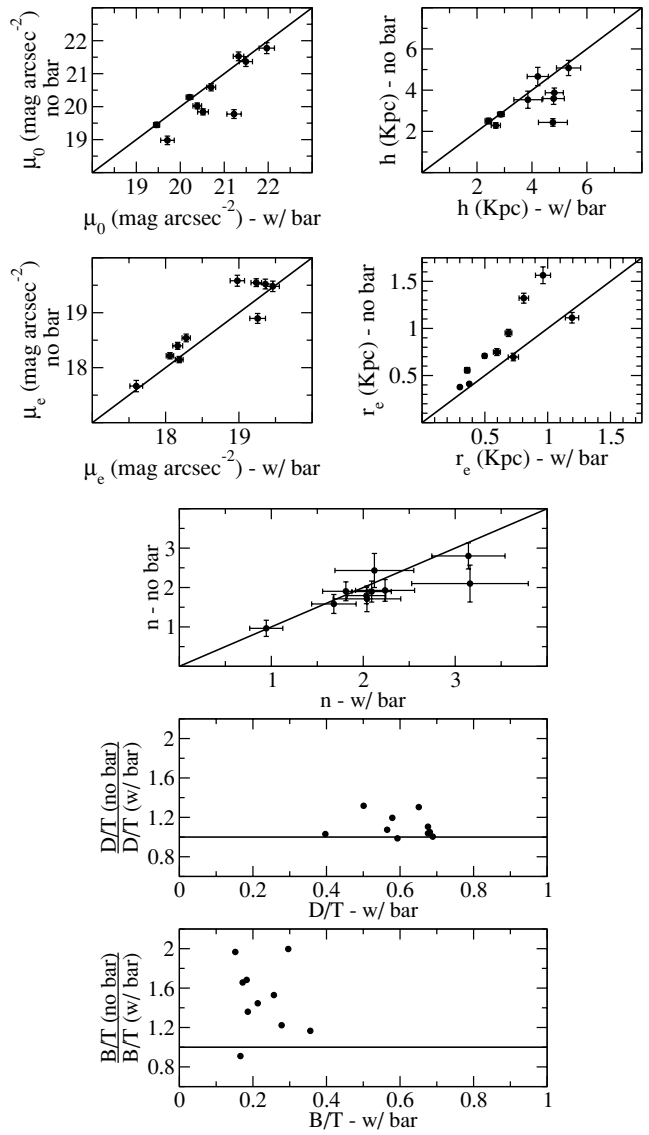

Figure 9. Structural parameters of discs and bulges, as estimated when bars are not included in the models, plotted against the same parameters when bars are taken into account. The two bottom panels show the relative overestimation of the disc-to-total and bulge-to-total luminosity fractions when bars are neglected, plotted against the corresponding parameters when the models include bars. The solid lines depict a perfect correspondence. This analysis excludes the five galaxies in the sample for which the AGN contribution has to be modelled, to avoid complicating the interpretation of the results. It shows that when bars are ignored, discs tend to assume steeper luminosity profiles, and bulges get bigger, in a way to accommodate the light from the bar. The effect is stronger for bulges: the bulge luminosity fraction can be overestimated by a factor of 2.

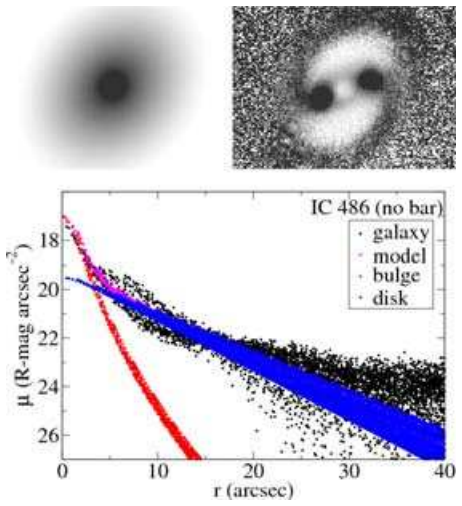

Figure 10. Results from the *R*-band image decomposition of IC 486 when the bar is not included in the model. Top left: total model image; top right: residual image; bottom: surface brightness profiles of the galaxy and the models. The images and the panel shown are similar to the corresponding ones in Fig. 1, and these should be compared in order to assess the effects of neglecting the bar. When the bar is not taken into account in the fitted model, the disc acquires a steeper profile, with a brighter central surface brightness, while the effective radius of the bulge grows. The resulting bulge-to-total and bulge-to-disc ratios get higher by 45 and 21 per cent, respectively. These changes are reflected in the residual image: the bulge model absorbs the inner part of the bar, and the brightened bulge and disc models produce strong negative residuals.

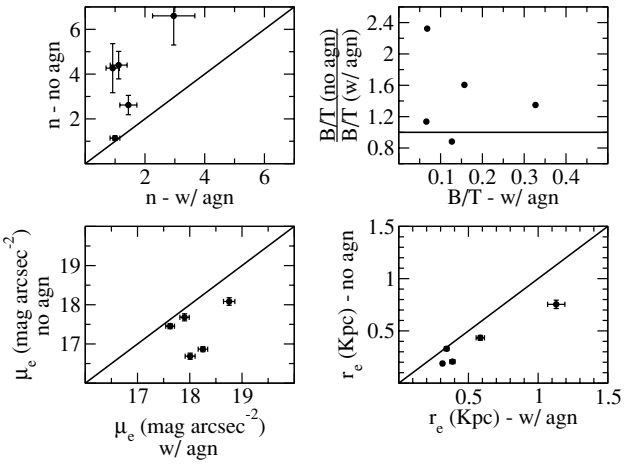

Figure 11. Structural parameters of bulges, and the relative overestimation of the bulge-to-total luminosity ratio, as estimated when AGN are not accounted for in the models, plotted against the corresponding parameters when AGN are taken into account. The solid lines depict a perfect correspondence. It is clear that, due to the concentrated light from the AGN, the bulge parameters cannot be reliably retrieved for galaxies hosting bright AGN if its contribution is not modelled. In this case, bulges tend to become smaller and more luminous. The Sérsic index of the bulge is the most affected parameter and can be overestimated by a factor of 4. The bulge luminosity fraction can be overestimated by a factor of 2.

cannot be reliably retrieved for galaxies hosting bright AGN if its contribution is not modelled.

In this study, the decision on whether or not to include an AGN component in the model was essentially based on the galaxy surface brightness profile and the AGN classification. A cuspy profile in a galaxy hosting an AGN indicates that the AGN contribution has to be taken into account. For larger studies, it would be interesting to have a way to predict if a galaxy needs the AGN component in the fit, without having to inspect the galaxy surface brightness profile. In principle, one would include the AGN model if the galaxy is a type 1 AGN. For one of the type 1 AGN galaxies in the sample, however, the AGN component was not needed. This might not be a matter of too much concern, though, as the code brought down the AGN contribution to the total galaxy light to negligible values,

when the first fit tried included this component. The resulting fit was not substantially different from the final fit, with the AGN removed from the model. On the other hand, weaker AGN, like in NGC 4579, might need an AGN component for an accurate fit, but, as shown above, the effects of neglecting the AGN in the fit to this galaxy are small. It thus seems that the fitting procedure is quite robust in deciding how important is the AGN contribution to the galaxy light distribution. This likely results from the fact that the AGN model contains only one free parameter, its peak intensity, plus one fixed parameter, the FWHM of its profile, which is given by the seeing FWHM. This suggests that it might not be too harmful, at least statistically, if an AGN component is included in the fits of all galaxies classified as AGN, provided that the input values for the bulge parameters given at the initial set-up of the fit are reasonable. A more appropriate procedure could be to evaluate the effects of dust obscuration in the centre of the galaxy, since heavily obscured AGN probably do not need to be modelled. With this aim, parameters such as the column density of absorbing hydrogen and the ratio between far-IR and optical or ultraviolet luminosities could be useful.

3.8 The light from spiral arms

By inspecting the original and residual images in Fig. 1, it is possible to see that many of the galaxies in the sample have bright spiral arms, which, in some cases in fact, appear to be a dominant component. Should these be taken into account in the image decompositions? To answer this question, one must first keep in mind that, to produce Fig. 1, the original images were displayed in a logarithmic scale, thus emphasizing structures with low surface brightness. Furthermore, the residual images were displayed with a very narrow dynamic range, also in order to point out faint, residual substructures. Thus, at least from a qualitatively viewpoint, the impression that the spiral arms might be a dominant component in these galaxies can be possibly wrong (at least in some cases), and results from the approach often used to render galaxy images and residual images.

A possible way to quantify what is the fraction of the galaxy light that comes from the spiral arms involves using the residual images. To this end, I produced new residual images, which were made by subtracting the model image from the original image (rather than dividing the latter by the former, as done before). The mean pixel value and the corresponding standard deviation were calculated within a region comprising the whole galaxy, i.e. from the centre to where the spiral arms end, as seen in the residual image. The mean value is always close to zero, which reveals an important aspect of the fitting procedure and the residual images: when fitting the disc component to a galaxy with spiral arms, the code tries to minimize the deviation between the galaxy and the model, thus creating an average disc model, which, on the one hand, accounts for at least part of the light that comes from the arms, and, on the other hand, produces slightly negative residuals in the interarm region. These negative residuals can be seen in Fig. 1, and should not be confused with the much more negative residuals discussed in Section 3.5. The important point is thus that at least part of the light from the spiral arms is already accounted for in the disc component of the model. With the residual images one can thus quantify how much light is in excess and was not included in the model. This was done by dividing the mean pixel value within the galaxy region in the residual image by the corresponding value in the original image, after statistically eliminating pixels with exceedingly negative values (i.e. more than three times the standard deviation – it turned out that this procedure does not significantly change the results). This was done for all galaxies, except NGC 2110, 2911 and 4267, where no conspicuous spiral arms are seen. No systematic or significant difference is seen when comparing the results from the *R*-band and the *V*-band images, but since the former have higher signal-to-noise ratio I consider the results from these images more reliable to discuss this issue. For IC 486, NGC 4477, 4593 and 5850, it was not possible to obtain a reliable value, i.e. the excess light is consistent with being zero, or at least only a tiny fraction of the total galaxy light ($<$0.1 per cent). For most galaxies the excess light is $\approx$1–2 per cent of the total galaxy light. For three galaxies the excess light is significant: NGC 4303 (10 per cent), NGC 4314 (4 per cent) and NGC 5383 (4 per cent).

Thus, these results suggest that, for most disc galaxies, the inclusion of a spiral arm component in the model is not a fundamental issue, and that the fraction of stellar mass contained within the spiral arms is too small, especially considering that the average mass-to-light ratio of the young stars in the arms is likely to be substantially lower than that in the remaining of the disc and the galaxy. Nevertheless, for some disc galaxies, particularly those with late morphological types, this fraction might be relatively important. A fully satisfactory approach to tackle this issue would thus be to include a spiral arm component in the model, resorting to e.g. Fourier techniques. One would then be able to answer more adequately what is the fraction of the disc and galaxy stellar mass that resides in spiral arms. This is, however, beyond the scope of this study.

4 DECOMPOSITION OF REDSHIFTED IMAGES

Recently, research on the structural properties of galaxies has shifted the main focus from the very nearby Universe to samples of more distant galaxies, as described in the Introduction, provided by surveys such as the SDSS (see e.g. ongoing work in Gadotti & Kauffmann 2007). This makes possible to carry on statistically significant analyses and, in some such studies, evaluate how the structure of galaxies changes with time. In many of these studies, however, the physical spatial resolution achieved in the galaxy images is substantially lower than what can be routinely achieved for nearby galaxies. It is thus most relevant to ask what impact such diminished resolution can have on the results. In addition, given the results from the previous section, one can ask whether bar and AGN components are still needed in the models when pushing to such low-resolution regimes. These questions are addressed in this section.

4.1 Fitting low-resolution images

To examine the effects of using low-resolution images for galaxy image decomposition, the original images used above were artificially redshifted to $z = 0.05$, which is $\approx$10 times farther than the actual location of the galaxies. This was done by demagnifying the images by the appropriate factor using the task MAGNIFY in IRAF, keeping the pixel angular size. In order to have the same resolution in all redshifted images, these were also convolved with a circular Gaussian, using the task GAUSS, in such a way that the final resolution is 1.5 arcsec, taking into account the resolution in the original image. This is the median seeing FWHM in the SDSS and, at $z = 0.05$, corresponds to a physical spatial resolution of $\approx$1.5 kpc. Such a resolution is typical in other works as well (e.g. Allen et al. 2006), and is what can be achieved at $z \sim$ 1–2 in images from the *Hubble Space Telescope* (*HST*), or from ground-based telescopes with adaptive optics. Thus, the following results have a broad applicability, being relevant to studies of the structure of galaxies in both the local Universe, like the ones just mentioned, and at higher redshifts, such as COSMOS (e.g. Koekemoer et al. 2007) and SINS

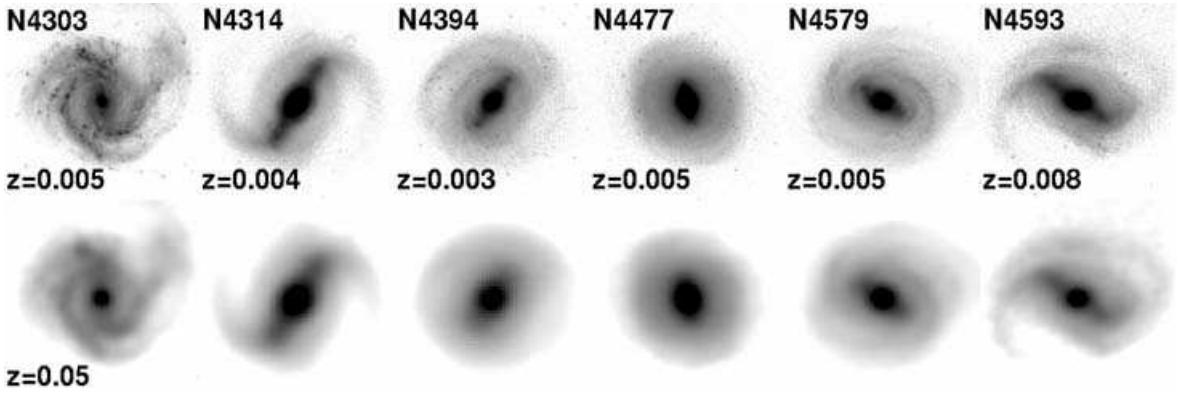

Figure 12. Comparison between the original images (top row) and artificially redshifted images (bottom row) for six galaxies in the sample, as indicated. The redshifted images simulate how the galaxies would look like if located at a redshift $z = 0.05$, i.e. ≈10 times farther than their actual location, and observed with a seeing of 1.5 arcsec.

(e.g. Genzel et al. 2006). A comparison between the original and redshifted images proves very instructive. This is done in Fig. 12. Features such as the star-forming knots and dust lanes in NGC 4303 are completely smoothed out, and only a hint of the spiral arms in NGC 4394 and the bar in NGC 4477 can be seen at low resolution.

The same procedures applied during the fitting of the original images were repeated with the redshifted images. Because of the larger uncertainties in the images of NGC 4151, 4665 and 5850, these galaxies were excluded from this analysis. It should be noted that, to allow a fair comparison between the results from both sets of images, the results obtained with the original images were not used to constrain the fitting of the redshifted images. In Fig. 13, the structural parameters of discs and bulges, and the bulge, disc and bar luminosity fractions, as determined with the redshifted images, are compared with the same parameters as obtained with the original images. For a proper comparison with the original images, the scalelengths from the redshifted images are scaled back to the original galaxy distance. One sees a very good agreement in what concerns the disc parameters and the disc and bar luminosity fractions. The agreement is also quite reasonable for the effective surface brightness of the bulge, but less so for its effective radius, Sérsic index and luminosity fraction. To understand better why some bulge parameters were not satisfactorily retrieved, the bulges were separated according to their effective radius in the redshifted images. Thus, in the corresponding panels in Fig. 13, filled circles refer to those galaxies where the ratio of the effective radius of the bulge in the redshifted image to the seeing radius (0.75 arcsec) is between ≈1 and ≈2; the empty circles correspond to those galaxies where this ratio is between ≈0.8 and ≈0.9 and the red points correspond to those galaxies where it is between ≈0.4 and ≈0.6. Clearly, the worst discrepancies almost always occur when the effective radius of the bulge is considerably small compared to the seeing radius. When the former is similar or larger than the latter the agreement between the results from original and redshifted images is somewhat improved.

Fig. 13 also shows lines that are linear regressions to the data points. The parameters that describe these lines, and their statistical uncertainties, and the corresponding correlation coefficients are shown in Table 4. Although the sample is relatively small, from these fits it is possible in principle to evaluate if there are systematic effects in the results in the low-resolution regime, and which structural parameters are most robust. Within the uncertainties, one sees that there seems to be no systematic effects in the determination of μ_0, h, D/T and Bar/T, and thus these parameters can be determined very reliably, in particular the central surface brightness of the disc, μ_0. As expected, bulge parameters are the most affected, even after removing those with r_e small compared to the seeing radius. There seems to be a systematic effect in μ_e, in the sense that bulges fainter than ≈18.5 R mag arcsec^{-2} are retrieved with a somewhat brighter μ_e when using the redshifted images. Similar effects seem to happen with r_e and n: the redshifted images provide smaller bulges if r_e is larger than about 6 arcsec, and less centrally concentrated bulges if n is greater than around 2. Note, however, that the typical 1σ error given by BUDDA for n is ≈0.5, which is quite big considering the full range covered by this parameter (e.g. here only from ≈1 to ≈3). This complicates the use of the bulge Sérsic index for a quantitative morphological classification of galaxies. To this aim, the bulge-to-total ratio seems to be a more robust parameter, since it shows the highest correlation coefficient amongst the bulge parameters. It also shows, however, a somewhat clearer systematic effect: bulge-to-total ratios recovered in the low-resolution regime are systematically larger than those estimated with the original images. Nevertheless, it is possible to suggest a mean correction from the data in Table 4. The corrected B/T, as a function of the estimated B/T (estimated in a low-resolution regime), is given by

$$\mathrm{B/T_{corr}} \approx 1.124 \times \mathrm{B/T_{est}} - 0.090. \quad (5)$$

From the data in Fig. 13, one sees that the average overestimation of B/T, due only to the low physical spatial resolution, is ≈5 per cent of the galaxy total luminosity. This light fraction, of course, has to be redistributed to the other galactic components. Although, as mentioned above, D/T and Bar/T do not show statistically significant systematic effects, one sees that most points in the corresponding panels in Fig. 13 lie close to, but below the perfect correspondence line, which makes this picture globally consistent. It is worth stressing again, though, that these assessments are based on a small sample and must be used with this caveat in mind.

4.2 The effects of neglecting bars and bright AGN at low resolution

Using the original images, we have seen that if one does not include bars and AGN in the models, when fitting galaxies that clearly host such components, the determination of the structural parameters can be severely affected. However, it is not clear if this is still true when the resolution of the images used is relatively poor. Given that finer

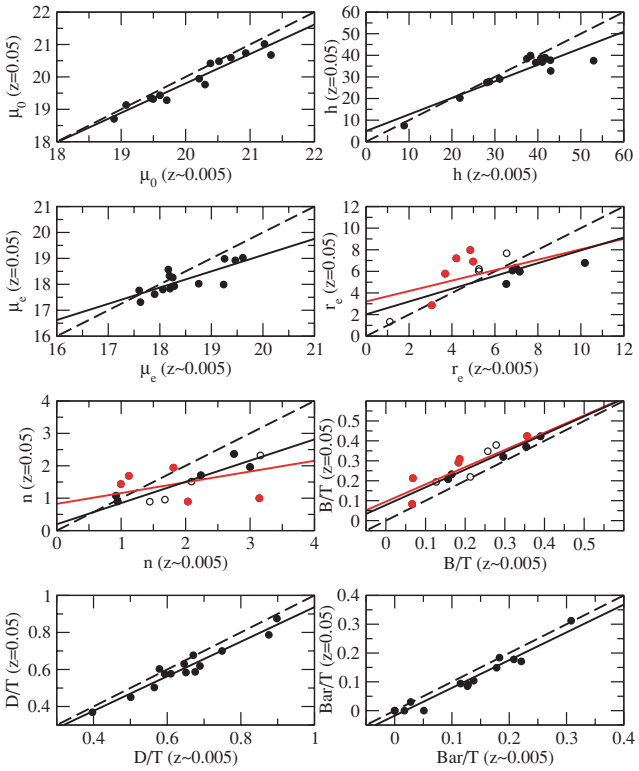

Figure 13. Structural parameters of discs and bulges, and bulge, disc and bar luminosity fractions, as determined with the redshifted images, plotted against the same parameters obtained with the original images. The dashed lines indicate a perfect correspondence. Luminosity parameters are in units of mag arcsec^{-2} and scalelengths in arcsec. For a proper comparison with the original images, the scalelengths from the redshifted images are scaled back to the original galaxy distance. For r_e, n and B/T, filled circles correspond to those galaxies where the effective radius of the bulge in the redshifted image is larger than the seeing radius, the empty circles correspond to those galaxies where it is similar to the seeing and the red points correspond to those galaxies where it is smaller than the seeing. The solid lines are linear fits to the data. For r_e, n and B/T, the red lines are fits to all data points, while the black lines correspond to fits where the red points were excluded. The parameters obtained from these linear regressions are shown in Table 4. One sees that, in general, structural parameters can be reliably retrieved through image fitting even in the low-resolution regime. Nevertheless, bulge parameters are prone to errors if its effective radius is small compared to the seeing radius, and might suffer from systematic effects.

details are smoothed out in this case, one expects these effects to be less significant, but do they completely disappear? To verify that, a similar exercise as done with the original images was repeated with the redshifted images. Thus, I selected three of the 10 barred galaxies in the sample with no conspicuous AGN component, which have a reliable original image and corresponding fit, and span a relatively wide range in bar luminosity fraction, and fitted a model to their redshifted images containing only bulge and disc. As in Section 3.6, the ellipticity and position angle of the bulge were kept fixed at the values found in the first fit, with the complete model, to the redshifted image, minimizing the effects caused by the absence of a model for the bar. Since the major effects of neglecting the bar are on the effective radius of the bulge and the bulge luminosity fraction, the analysis is focused on these parameters. Table 5 compares, for each of these galaxies, the effective radius of the bulge and the bulge luminosity fraction, as determined with the original images and the redshifted images, with and without a bar in the model.

Table 4. Linear regression results for Fig. 13.

Parameter	cc	a	b
μ_0	0.97	0.91 ± 0.07	1.62 ± 1.43
h	0.91	0.77 ± 0.10	4.95 ± 3.63
μ_e	0.79	0.63 ± 0.14	6.59 ± 2.62
r_e^*	0.58	0.48 ± 0.19	3.21 ± 1.14
$r_e^\star$	0.79	0.59 ± 0.17	2.02 ± 1.15
n^*	0.51	0.33 ± 0.16	0.83 ± 0.34
$n^\star$	0.92	0.65 ± 0.11	0.19 ± 0.23
B/T*	0.91	0.86 ± 0.11	0.10 ± 0.03
B/T*	0.93	0.89 ± 0.13	0.09 ± 0.03
D/T	0.97	0.93 ± 0.07	0.00 ± 0.05
Bar/T	0.98	0.96 ± 0.06	-0.02 ± 0.01

Parameters obtained from the linear regressions in Fig. 13: cc is the correlation coefficient, a is the slope of the line and b its intercept. Thus, the fitted line to, e.g. μ_0, can be written as $y = 0.91(\pm0.07)x + 1.62(\pm1.43)$. Uncertainties quoted are 1σ errors from the fit. Luminosity parameters are in units of mag arcsec^{-2} and scalelengths in arcsec. For r_e, n and B/T, parameters with * appended correspond to fits using all data points, whereas those with * appended correspond to fits where the data points deemed unreliable were excluded.

One sees that, in cases that bars are prominent, like in NGC 4314 and 4394, the overestimation of these parameters when the bars are neglected occurs using the redshifted images as much as when the original images were used (see also Fig. 14). The relative change in the B/T value after omitting the bar is similar in both the original and redshifted images. The change in r_e is even more pronounced in the latter (by a factor of $\approx$2), and this might be due to the fact that the geometrical properties of the bulge are in this case substantially affected by the PSF, which tends to make the bulge rounder, making it harder to constrain its properties. For a galaxy with a less prominent bar, like NGC 4477, these effects are still present, albeit with a reduced strength.

Similarly, three of the five galaxies in the sample which were originally fitted with an AGN component in the model were selected, and their redshifted images fitted without the AGN. Since the major effect of neglecting the AGN is on the Sérsic index of the bulge, the analysis is focused on this parameter. Table 6 compares, for each of these galaxies, the Sérsic index of the bulge, as determined with the original images and the redshifted images, with and without the AGN in the model. One sees that the overestimation of the Sérsic index, that happens when not accounting for the AGN contribution when fitting the original images, does not occur in the low-resolution regime, not even in the case of NGC 4593, which has a very luminous AGN (see Fig. 14).

5 IMPLICATIONS FOR STUDIES ON THE STRUCTURAL PROPERTIES OF GALAXIES

Image fitting of galaxies is a complex endeavour, especially when dealing with galaxies rich in structure, such as barred galaxies. Thus, the fact that with the structural parameters obtained here one can reproduce previously known correlations (Figs 2, 3 and 4), and the agreement between these parameters and those from similar studies in the literature (Section 3.3, Fig. 5) are very encouraging. Likewise, the fact that the structural parameters obtained with the redshifted images agree with those obtained with the original images, as seen in the previous section, gives support to studies based on more distant galaxies, if the effective radius of the bulge is not small compared

Table 5. Bar effects on r_e and B/T at different resolutions.

		$z \approx 0.005$				$z = 0.05$			
Galaxy	Bar/T	r_e (Bar)	r_e (no Bar)	B/T (Bar)	B/T (no Bar)	r_e (Bar)	r_e (no Bar)	B/T (Bar)	B/T (no Bar)
(1)	(2)	(3)	(4)	(5)	(6)	(7)	(8)	(9)	(10)
NGC 4314	0.308	10.9	16.6 (52 per cent)	0.296	0.591 (100 per cent)	6.8	14.8 (118 per cent)	0.320	0.618 (93 per cent)
NGC 4394	0.138	4.2	5.3 (26 per cent)	0.186	0.253 (36 per cent)	7.2	10.5 (46 per cent)	0.309	0.375 (21 per cent)
NGC 4477	0.128	4.9	7.1 (45 per cent)	0.183	0.308 (68 per cent)	6.9	8.2 (19 per cent)	0.291	0.370 (27 per cent)

Column (1) gives the galaxy name and column (2) shows the estimated bar luminosity fraction. Columns (3) and (4) show the effective radius of the bulge, r_e, with and without a bar in the model, respectively. Similarly, columns (5) and (6) show the estimated bulge luminosity fraction, with and without a bar in the model. The latter five columns refer to the original galaxy images. Columns (7) to (10) are similar to columns (3) to (6) but refer to the artificially redshifted images. The effective radius is in arcsec and, for the redshifted images, scaled back to the original galaxy distance. The values in parentheses give the relative change in the parameter when omitting the bar.

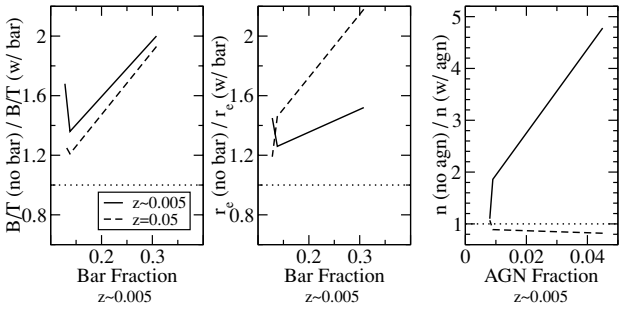

Figure 14. Left and central panels: overestimation of the bulge-to-total luminosity ratio and the effective radius of the bulge, as a function of the bar luminosity fraction, when there is no bar in the fitted model, relative to the same parameter when the bar is taken into account. Right: overestimation of the bulge Sérsic index as a function of the AGN luminosity fraction, when the AGN light is not modelled, relative to the same parameter when the models include AGN, for galaxies where an AGN component is included in the fit of the original images (see Section 4). The solid lines refer to the original images while the dashed lines refer to the artificially redshifted images. The dotted lines indicate no change in the parameters. This figure is a graphical representation of Tables 5 and 6. It shows that the overestimation of B/T when ignoring bars, as seen in Section 3.6, is still significant even in the low-resolution regime, but has its strength reduced in this regime if the bar is weak. The corresponding overestimation of r_e is even considerably worse in the low-resolution regime if the bar is not too weak. Furthermore, it also shows that the overestimation of n, when the AGN contribution is not taken into account, as seen for the original images in Section 3.7, is completely absent in the low-resolution regime.

to the PSF, and the physical spatial resolution is 1.5 kpc or better. With the work presented here one cannot conclude on whether a similar agreement emerges if the resolution is poorer. A word of caution should be given, however: the redshifted images were fitted and checked individually, and automated procedures usually applied to large samples normally lead to larger uncertainties. Furthermore, only the effects of a lower spatial resolution in the images of more distant galaxies are mimicked in the redshifted images, but other issues, such as dimming and wavelength shifting, might as well be relevant, especially if reaching $z \sim 1$.

The bar luminosity fraction of the galaxies in the sample range, in the *R* band, from around 2 to 30 per cent, with a median value of ≈14 per cent and standard deviation of ≈8 per cent. Similar results are obtained from the *V*-band images. This broadly agrees with the findings of Gadotti & Kauffmann (2007) with a sample of about 100 barred galaxies, namely, $0.01 \leqslant \mathrm{Bar/T} \leqslant 0.3$, with a median value ≈10 per cent (see also Reese et al. 2007). This means that the effects of not modelling the bars in barred galaxies, seen in Section 3.6, should be typical. We saw that the most affected parameters are the effective radius of the bulge and the bulge-to-total luminosity ratio, both being significantly overestimated. We also saw that these effects hold in the low-resolution regime (Section 4.2, Table 5 and Fig. 14), provided that the bar is prominent enough. For NGC 4477, the galaxy with the least prominent bar, amongst the galaxies with which this analysis was done, with $\mathrm{Bar/T} = 0.128$, these effects are substantially less pronounced in the redshifted images, compared to the original images. Thus, even at low resolution, these effects are important for at least about half of the barred galaxies, i.e. roughly about 1/3 of disc galaxies. On the other hand, it seems reasonable to conclude that, for galaxies with Bar/T below ≈0.1, and in the low-resolution regime, the effects of neglecting the bar are within the uncertainties. Nevertheless, even for these galaxies, such effects should result in a systematic overestimation of r_e and B/T.

Evidently, regardless of image resolution, ignoring bars in barred galaxies affects results on the stellar mass budget in the Universe, i.e. the distribution of mass in stars in the different galactic components. When bars are not somehow taken into account, the amount of mass in stars in bulges and discs is overestimated, and the excess is an indication of the amount of mass in stars that reside in bars. Using

Table 6. AGN effects on the bulge Sérsic index at different resolutions.

		$z \approx 0.005$		$z = 0.05$	
Galaxy	AGN/T	n (with AGN)	n (without AGN)	n (with AGN)	n (without AGN)
(1)	(2)	(3)	(4)	(5)	(6)
NGC 4303	0.008	1.0	1.1	1.4	1.5
NGC 4579	0.009	1.4	2.6	0.9	0.8
NGC 4593	0.045	0.9	4.3	1.1	0.9

Column (1) gives the galaxy name, while column (2) shows the estimated AGN luminosity fraction. Column (3) shows the bulge Sérsic index when the AGN is included in the model, while column (4) shows the same parameter when the AGN is not taken into account. The latter three columns refer to the original galaxy images. Columns (5) and (6) are similar to columns (3) and (4), respectively, but refer to the artificially redshifted images.

the original images, we have seen that the average overestimation of the bulge and disc luminosity fractions is, respectively, 50 and 10 per cent. Applying image decomposition techniques to a sample of more than 10^4 galaxies, Driver et al. (2007) estimated that the $z \approx 0$ stellar mass content in classical bulges and discs is 26 ± 4 and 58 ± 6 per cent, respectively (see also Tasca & White 2005). They also find that the stellar mass content in elliptical galaxies is 13 ± 4 per cent. Bars are not taken into account in the fitted models, which contain only bulge and disc. These authors made a thorough quality control, removing a significant fraction of the fits, which were deemed poor. Thus, one could argue that barred galaxies have not passed quality control. However, it is usually the case that, even when there is no bar in the model, when fitting a barred galaxy, one gets an acceptable (though wrong) fit, essentially because the bulge model is distorted, trying to accommodate the bar light, as shown in Section 3.6. Hence, we can use their results to obtain a rough estimate of what can be the stellar content in bars, assuming that the biases produced by ignoring bars, as found in Section 3.6, can be used in this case to obtain the true bulge and disc luminosity fractions. If one uses the average result from equation (5), to correct the bulge fraction due to the effects of low spatial resolution, as discussed above (the physical spatial resolution of the images used by Driver et al. is on average very similar to that of the redshifted images I use here), and assumes that the fraction of barred galaxies, considering only disc galaxies, is $\approx$70 per cent, then the stellar content in classical bulges and discs is found to be $\approx$13.5 and $\approx$58.5 per cent, respectively, and the stellar content in bars is $\approx$12 per cent.[2] Incidentally, this fraction of the stellar mass in discs is still very similar to that given by Driver et al. For bulges, however, the corresponding difference is $\approx 3\sigma$, considering their error estimate. Bulges, discs and bars can have different mass-to-light ratios and this is not taken into account here, adding more uncertainty to these estimates. Nevertheless, they open up the possibility of bars being as important as classical bulges and ellipticals in what concerns their stellar mass content in the local Universe.

As discussed in Section 3.8, the stellar mass content in spiral arms seems to be small, at least for early-type disc galaxies, and might not increase significantly the stellar mass content of discs; this raise might well be within the errors. Nevertheless, we have seen that some galaxies do have very conspicuous spiral arms, which might contain a non-negligible fraction of the stellar mass of the galaxy. Thus, two related questions, which are relevant to studies on galactic structure and star formation, and whose answers are not clear, emerge from this discussion: (i) what is the fraction of the stellar mass of the disc of a galaxy with prominent spiral arms that resides within the arms, and (ii) what is the fraction of disc galaxies that host such prominent spiral arms. With reliable answers to these questions one would be able to properly include spiral arms as another separate constituent of the stellar mass budget.

It was shown, in Section 3.7 (Fig. 11), that not taking into account the contribution from bright AGN to the light distribution in the central region of a galaxy can lead to severe errors in the bulge parameters. In particular, the Sérsic index of the bulge can be significantly overestimated.[3] Thus, one could, in principle, devise a methodology to identify AGN using only imaging data, through these effects. The main advantage over current methods, which use spectroscopy data, would be that imaging usually requires much less telescope time and/or smaller telescopes. One could fit the galaxy image (aiming to find AGN, it could be that fitting only the surface brightness profile is enough) with and without the AGN in the model. If the Sérsic index of the bulge, estimated in the latter fit, is larger than the one obtained in the former, over the uncertainties (which are usually ± 1 for this parameter), this would be an indication of the presence of an AGN. However, we saw that only bright, type 1 AGN produce such effects. Furthermore, there could be large uncertainties due to the degeneracy in the possible solutions. For instance, a classical bulge with $n = 3$ could be misidentified as a pseudo-bulge, with $n = 1$, containing an AGN. In addition, as seen in Section 4.2 (Table 6 and Fig. 14), if the resolution is not sufficient, the effects of the extra light from AGN are negligible. Not surprisingly, as opposed to bars, the AGN contribution is completely smeared out by the PSF in the low-resolution regime. Such a methodology would then be severely prone to errors.

Notably, the effects of ignoring bars and AGN, and the effects of having images with low resolution, all affect bulges more substantially than discs. Partly, this might be due to the fact that a simpler function, an exponential, is used to describe the disc luminosity profile, as compared to the Sérsic function, used to describe the bulge luminosity profile. A simple exponential function, however, might not be, in many cases, the best choice to fit discs. The results for NGC 4608 and 5701 in Section 3.5 are clear instances, even if, perhaps, extreme cases. In e.g. Erwin, Beckman & Pohlen (2005, and references therein) one finds a number of cases in which the luminosity profile of the disc can be better reproduced by a double exponential function. It is worth noting that in BUDDA v2.1 it is possible to use such a function to fit discs.[4] Nevertheless, discs are the more extended luminous galactic component and this might also partially explain the robustness of the disc fits. The results obtained in this study suggest that, in general, the structural parameters of discs are those which are more reliably determined.

6 SUMMARY AND CONCLUSIONS

I presented the results of image fitting to a sample of 17 nearby galaxies, imaged in the *V* and *R* broad-bands, including the structural parameters of bulges, discs and bars. The light from bright AGN was taken into account when needed. A number of tests is performed to verify the reliability of such techniques when bars and AGN are not included in the models, and when the images have a relatively poor physical spatial resolution, which is usually the case of studies on large samples of more distant galaxies. The main results from this work can be summarized as follows.

(1) The ellipticity of bars, when measured as the peak in the ellipticity profile from ellipse fits to the galaxy image, is underestimated,

[2] To get to these numbers, first one has to remove 5 per cent from the original stellar content in bulges, given by Driver et al., since this is the average overestimation of B/T due only to the low physical spatial resolution in the images, and add that 5 per cent to the original content in discs (one could distribute this fraction between discs and bars, but let's be conservative). Then, multiply the assumed fraction of barred galaxies, 70 per cent, by the average overestimation of B/T due to the absence of bars in the models, 50 per cent, and multiply the result by the bulge content just found, 21 per cent. This results in $\approx$7.5 per cent, which also has to be removed from this bulge content and added to the bar content, which was, up to now, zero. Similarly, for the discs: $70 \times 10 \times 63 \approx 4.5$ per cent, which has to be removed from the disc content and added to the bar content. If one deems the first step unnecessary, the stellar mass content in bulges, discs and bars change to 17, 54 and 13 per cent, respectively.

[3] Given enough spatial resolution, as in *HST* images of nearby galaxies, other central components, like nuclear star clusters, can induce similar effects.

[4] See http://www.mpa-garching.mpg.de/~dimitri/budda.html

on average, by ≈20 per cent. To obtain the true bar ellipticity, the contribution from the axisymmetric components (most importantly the disc) to the galaxy image has to be considered.

(2) Modelling of galaxy images is a reliable tool to determine the structural parameters of bulges, discs and bars, even in a low-resolution regime, i.e. at least up to the point where the physical spatial resolution in the image is 1.5 kpc, but the bulge parameters are only trustworthy if its effective radius is not small compared to the PSF radius. The disc parameters are the most robust, in particular the disc central surface brightness. The luminosity fractions of bulges, discs and bars are also recovered very reliably. The bulge-to-total fraction, however, has to be corrected for a systematic effect, using equation (5). The bulge-to-total fraction is a favoured parameter to be used for quantitative morphological classification of galaxies, as opposed to the bulge Sérsic index, since the latter has large uncertainties compared to its usual dynamic range.

(3) If bars are not modelled, when fitting barred galaxies, the structural parameters of bulges and discs can be severely compromised, particularly the bulge effective radius. Furthermore, the disc-to-total luminosity ratio is overestimated, on average, by ≈10 per cent, and the bulge-to-total luminosity ratio is overestimated, on average, by ≈50 per cent. These effects are still significant in the low-resolution regime, albeit with a reduced impact, in this case, for weaker bars.

(4) If the light from bright, type 1 AGN is not modelled, when fitting their hosts, the structural parameters of bulges can be severely compromised, particularly the bulge Sérsic index. The bulge-to-total luminosity ratio can be overestimated by a factor of 2. However, in the low-resolution regime, the AGN contribution is smeared out by the PSF and these effects are absent.

(5) Using the results concerning the biases in the estimation of the bulge and disc luminosity fractions, due to low spatial resolution and the non-inclusion of bars in the photometric models, it is possible to correct the stellar mass budget in the local Universe, as found in the literature, to take into account the mass in stars that reside in bars. The results are as follows: the stellar content in classical bulges and discs is found to be ≈13.5 and ≈58.5 per cent, respectively, and the stellar content in bars is ≈12 per cent. None the less, these are rough estimates and need to be confirmed by further studies, in particular, by the direct inclusion of bars in the models used to fit galaxy images in large samples.

ACKNOWLEDGMENTS

It is a pleasure to thank Guinevere Kauffmann and Lia Athanassoula for useful discussions and for comments on a first draft of this paper, which helped to significantly improve it, and Ronaldo de Souza for his help in the making of the new BUDDA version. Author would also like to thank an anonymous referee who contributed with insightful suggestions. DAG is supported by the Deutsche Forschungsgemeinschaft priority program 1177 ('Witnesses of Cosmic History: Formation and Evolution of Galaxies, Black Holes and Their Environment'), and the Max Planck Society.

REFERENCES

Allen P. D., Driver S. P., Graham A. W., Cameron E., Liske J., de Propis R., 2006, MNRAS, 371, 2
Athanassoula E., 1992, MNRAS, 259, 328
Athanassoula E., 2002, ApJ, 569, L83
Athanassoula E., 2003, MNRAS, 341, 1179
Athanassoula E., Misiriotis A., 2002, MNRAS, 330, 35
Athanassoula E., Morin S., Wozniak H., Puy D., Pierce M. J., Lombard J., Bosma A., 1990, MNRAS, 245, 130
Binney J., Tremaine S., 1987, Galactic Dynamics. Princeton Univ. Press, Princeton, NJ
Buta R., Laurikainen E., Salo H., Block D. L., Knapen J. H., 2006, AJ, 132, 1859
Caon N., Capaccioli M., D'Onofrio M., 1993, MNRAS, 265, 1013
de Jong R. S., 1995, PhD thesis, Univ. Groningen, the Netherlands
de Jong R. S., 1996, A&A, 313, 45
de Souza R. E., Gadotti D. A., dos Anjos S., 2004, ApJS, 153, 411
de Vaucouleurs G., de Vaucouleurs A., Corwin H. G., Buta R. J., Paturel G., Fouque P., 1991, Third Reference Catalog of Bright Galaxies. Springer-Verlag, New York (RC3)
D'Onofrio M., 2001, MNRAS, 326, 1517
Driver S. P., Allen P. D., Liske J., Graham A. W., 2007, ApJ, 657, L85
Elmegreen B. G., Elmegreen D. M., 1985, ApJ, 288, 438
Erwin P., 2005, MNRAS, 364, 283
Erwin P., Beckman J. E., Pohlen M., 2005, ApJ, 626, L81
Eskridge P. B. et al., 2000, AJ, 119, 536
Freeman K. C., 1970, ApJ, 160, 811
Gadotti D. A., de Souza R. E., 2003, ApJ, 583, L75
Gadotti D. A., de Souza R. E., 2005, ApJ, 629, 797
Gadotti D. A., de Souza R. E., 2006, ApJS, 163, 270 (GdS06)
Gadotti D. A., dos Anjos S., 2001, AJ, 122, 1298
Gadotti D. A., Kauffmann G., 2007, in Vazdekis A., Peletier R., eds, IAU Symp. 241, Stellar Populations as Building Blocks of Galaxies. Cambridge Univ. Press, Cambridge, p. 507
Gadotti D. A., Athanassoula E., Carrasco L., Bosma A., de Souza R., Recillas E., 2007, MNRAS, 381, 943
Genzel R. et al., 2006, Nat, 442, 786
Häussler B. et al., 2007, ApJS, 172, 615
Hubble E. P., 1926, ApJ, 64, 321
Hubble E. P., 1936, The Realm of the Nebulae. Yale Univ. Press, New Haven, CT
Huertas-Company M., Rouan D., Soucail G., Le Fèvre O., Tasca L., Contini T., 2007, A&A, 468, 937
Khosroshahi H. G., Wadadekar Y., Kembhavi A., 2000, ApJ, 533, 162
Koekemoer A. M. et al., 2007, ApJS, 172, 196
Kormendy J., 1977, ApJ, 218, 333
Kormendy J., Kennicutt R. C., 2004, ARA&A, 42, 603
Laurikainen E., Salo H., Buta R., Vasylyev S., 2004, MNRAS, 355, 1251
Laurikainen E., Salo H., Buta R., 2005, MNRAS, 362, 1319
Laurikainen E., Salo H., Buta R., Knapen J., Speltincx T., Block D., 2006, AJ, 132, 2634
Marinova I., Jogee S., 2007, ApJ, 659, 1176
Marleau F. R., Simard L., 1998, ApJ, 507, 585
Martinez-Valpuesta I., Knapen J. H., Buta R., 2007, AJ, 134, 1863
Moffat A. F. J., 1969, A&A, 3, 455
Möllenhoff C., Heidt J., 2001, A&A, 368, 16
Patsis P. A., Skokos C., Athanassoula E., 2003, MNRAS, 342, 69
Peng C. Y., Ho L. C., Impey C. D., Rix H.-W., 2002, AJ, 124, 266
Pignatelli E., Fasano G., Cassata P., 2006, A&A, 446, 373
Reese A. S., Williams T. B., Sellwood J. A., Barnes E. I., Powell B. A., 2007, AJ, 133, 2846
Sellwood J. A., Wilkinson A., 1993, Rep. Prog. Phys., 56, 173
Sérsic J. L., 1968, Atlas de Galaxias Australes. Observatorio Astronomico, Cordoba
Tasca L. A. M., White S. D. M., 2005, MNRAS, submitted (astro-ph/0507249)
Trujillo I., Aguerri J. A. L., Cepa J., Gutiérrez C. M., 2001a, MNRAS, 321, 269
Trujillo I., Aguerri J. A. L., Cepa J., Gutiérrez C. M., 2001b, MNRAS, 328, 977

This paper has been typeset from a TEX/LATEX file prepared by the author.